

# 3D Printed Clay Formwork for A Functionally Integrated Wall Construction

Master Thesis  
Department of Architecture  
TUM School of Engineering and Design  
Technical University of Munich

**Supervised by** Prof. Dr. sc. ETH Kathrin Dörfler, Gido Dielemans, M.Sc.  
TT Professorship of Digital Fabrication

**Submitted by** Zirui Huang  
Munich, 15.09.2022

# Abstract

In concrete construction, the production of formwork accounts for the largest percentage of cost. To be more economical, the most of the commercially available formwork systems today are based on standardized flat panels. Clay is a component of earth, which is the most important natural material, and it is available in most regions. If not sintered, clay can be recycled and reused very easily. With the availability and recyclability of the clay material, 3D printed clay formwork allows the formwork for bespoke concrete structures to be produced at very low cost. Research have demonstrated the possibility of 3D printed clay formwork and explored its design potentials with prototypes successfully fabricated in architectural scale. However, it still needs to be explored how a clay formwork larger than the range of a static robot can be printed using multiple mobile robots in an in-situ fabrication scenario. For that purpose, this thesis aims at developing a parametric workflow for designing print path models of 3D printed clay formwork in such a scenario.

Based on an analysis of challenges from robot, material and fabrication process in an in-situ clay formwork printing scenario, a parametric design workflow was developed to model the print paths of the clay formwork. A segmentation process has been implemented to tessellate the clay formwork into smaller tiles regarding the robot range, end-effector collision and the incremental printing and casting process. Stiffening features have been integrated into the print path model to support the clay formwork against its self-weight and the hydrostatic pressure from liquid concrete during printing and casting. Joints have been integrated to the print paths to ensure a stable interlocking between clay formwork tiles. The parametric workflow was then tested on two demonstrator geometries: column and wall. The feasibility of the development was evaluated by experimentally manufacturing the column in 1:1 scale.

The physical printing experiment succeeded in demonstrating the feasibility of manufacturing clay formworks with mobile robots. The parametrical workflow with segmentation, stiffening and jointing methods developed for the print path modelling have been proved to be valid. As an outlook, functionalities like prefabricated opening components can be integrated into the formwork tessellation as stay-in-place formworks and this technology can find architectural application. Furthermore, an initial experiment has been conducted to explore the possibility combination of clay formwork and earth casting, which could be a future research topic.

# Glossary

*In-situ fabrication:* Fabrication of structures directly at their final destination

*Mobile robot:* A robot arm mounted on a platform with mobility function.

*Hydrostatic pressure:* The pressure that is exerted by a fluid at equilibrium at a given point within the fluid, due to the force of gravity.

*Clay extrusion:* The process of pushing clay through a deposit tool with pressure.

*End-effector:* The device at the end of a robotic arm, designed to interact with the environment and perform tasks.

*Robot range:* The area that a robot's end-effector can reach.

*Robot relocation:* The repositioning of a mobile robot from one location to another.

*Print path:* Ordered list of points in space which a robot should follow.

*Frame:* Geometry defined by a base point and two orthonormal base vectors to determine the position and orientation of an object in space.

*Tessellation:* Covering of a surface using one or more geometric shapes, called tiles, with no overlaps and no gaps.

*Tile:* The geometric shape used to tessellate a surface. In this thesis also: a piece of a segmented clay formwork.

# Table of Contents

1. Introduction .....	7
2. State of the Art .....	7
3. Research Objective .....	9
4. Method .....	11
4.1. General .....	11
4.2. Segmentation .....	12
4.3. Stiffening .....	23
4.4. Jointing .....	28
5. Results .....	31
5.1. Case 1: Column .....	31
5.2. Case 2: Wall .....	37
5.3. Fabrication of The Column .....	41
6. Conclusio .....	47
6.1. Outlook .....	47
6.2. Discussion .....	48
7. Bibliography .....	49
8. Table of Figures .....	50

# 1. Introduction

In concrete construction, the production of formwork accounts for the largest percentage of cost. To be more economical, the most of the commercially available formwork systems today are based on standardized flat panels. Standardized formworks usually result in oversized concrete components, but the extra cost for bespoke formworks still outweighs the extra cost of concrete (Jipa and Dillenburger 2021).

Earth is the most important natural material, and it is available in most regions. Earth, when used as a building material, is often given different names. Referred to in scientific terms as loam, it is a mixture of clay, silt (very fine sand), sand, and occasionally larger aggregates such as gravel or stones (Minke 2021).

Clay is a component of earth. It is the most important raw material for many building components such as bricks and tiles. These components are produced by burning the clay. Burning the clay is a non-reversible process. Once is sintered, clay gains structural strength and becomes water resistant, however losing its recyclability. If clay is not sintered, it can be recycled and reused very easily. With the availability and recyclability of the clay material, 3D printed clay formwork allows the formwork for bespoke concrete structures to be produced at very low cost.

The clay extrusion process was first developed in the 2000s. In clay extrusion, clay is pushed through a deposition tool. Clay is printable because of the non-Newtonian shear-thinning rheology. Once the shear-inducing extruding process stops, the viscosity of the clay material decreases (Jipa and Dillenburger 2021). Layers of extruded clay cumulatively added on top of each other, gradually building up large objects. The deposition tool can be connected to a gantry system or a robotic arm, allowing non-standard geometries to be produced.

## 2. State of the Art

In 2015, XtreeE used 3D printed clay formworks for the first time to produce a concrete space truss (Jipa and Dillenburger 2021). In this project, to support the shape-giving geometry, a honeycomb supporting structure is also printed with clay. In addition, extra clay is filled into all the voids in the entire geometry's bounding box. The clay formwork is washed away after the concrete sets ("3D Concrete Printing Expands to World Construction" n.d.).

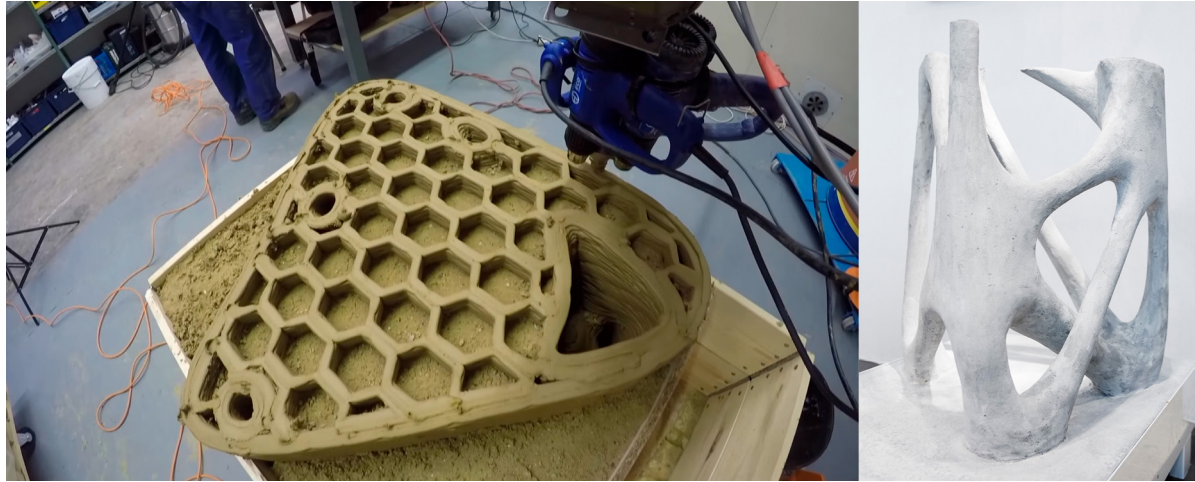


Figure 1: Clay formwork being printed (left). Prototype of a 3D lattice structure (right). (“3D Concrete Printing Expands to World Construction” n.d.)

In 2020, the “Cocoon” project at Taubman College proved the concept of 3d printed formwork for concrete casting by producing a complex concrete column with branching geometry at architectural scale. They used fast-setting concrete mixture in an incremental casting process, in which concrete works together with formwork to hold the structure. This allows a very thin clay formwork to reach a scale previously unachievable. The “Void Support” is a minimal surface supporting branching structures, the “Rib Support” improves the rigidity of formwork. Both supports were added into a continuous clay printing toolpath generation. (“Ruxin Xie - 21SU’ Cocoon” n.d.)



Figure 2: Incremental concrete casting process in “Cocoon” allows concrete to support the 3DP clay formwork (left). Concrete column “Cocoon” with branching geometry (right). (“Rcuxin Xie - 21SU’ Cocoon” n.d.)

In 2022, the master thesis “Growing Buttress” at Taubman College also explored 3d printed clay formwork by producing a concrete panel at architectural scale. Same as the incremental casting process of “Cocoon”, a print-cast-print process was used here to use the weight of concrete as stabilization elements. Buttresses were added to the formwork according to

hydrostatic simulation to balance the plasticity of clay. (“TEXT\_Qian Li and Kamon Nartnarumit - Taubman College Thesis 2022” n.d.) Video: (“3D PRINTED CLAY FORMWORK FOR CONCRETE CASTING - YouTube” n.d.) In another video from their channel, they were also exploring metal reinforcements for better jointing between different concrete casts in the print-cast-print process. (“Print-Cast-Print - YouTube” n.d.)



Figure 3: Clay formwork being printed on top of previous cast (left). (“Print-Cast-Print - YouTube” n.d.) Concrete being casted in 3d printed clay formwork (right). (“3D PRINTED CLAY FORMWORK FOR CONCRETE CASTING - YouTube” n.d.)

### 3. Research Objective

The research “Cocoon” and “Growing Buttress” demonstrated the possibility of 3D printed clay formwork and explored its design potentials. Also, the concept of using concrete as support has been proved to be especially important and useful for this process. Furthermore, this research proved that this technology can be applied to the fabrication of large structures at architectural scale.

However, in both research, a stationary fabrication setup was used to produce the structure. One major disadvantage of a stationary setup is that the maximal size of structure is limited by the size of fabrication setup. Take the “Growing Buttress” for example, a KUKA robot arm was used to produce the structure, therefore the size of the fabricated structure is limited by the reach range of the robot arm. Another disadvantage is that a stationary setup requires a lot of effort to transport to the building site and is difficult to relocate. A stationary fabrication setup is very well suited for prefabrication scenario, in which components are prefabricated in factories and assembled into structures on the building site. But on the other side of the picture, in-situ fabrication, where raw materials are directly built into structures on the building site, is not less common than prefabrication, especially in concrete construction.

In an in-situ fabrication scenario, structures are usually much larger than the reach range of one robot arm. This is where mobile robots become very handy and advantageous over large stationary setups because of their mobility. Even though one of them has a smaller reach

range compared to large robot arm in a stationary setup, they can extend their reach range by relocating and cooperating. In addition to that, their small size makes it easier for them to work on the building site around obstacles such as printing around reinforcement cages that are installed beforehand.

The research objective of this paper is to explore how a clay formwork larger than the static robot range can be 3D printed with multiple mobile robots in an in-situ fabrication scenario. The objective is broken down into the following steps:

- To understand the challenges of 3d printed clay formwork using mobile robots.
- To develop a parametrical workflow for the print path design of the clay formwork.
- To demonstrate print path design of the clay formwork with a physical prototype.

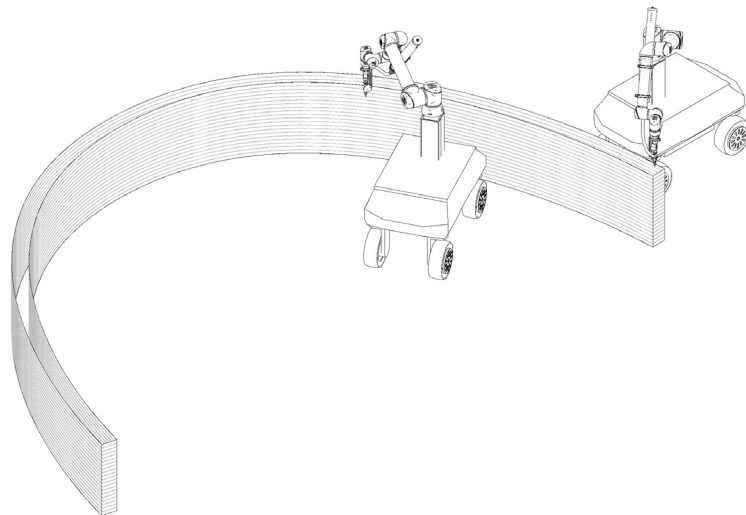


**Figure 4: In-situ clay formwork printing scenario.**

## 4. Method

### 4.1. General

This thesis approaches the objective by using a combination of analytical and experimental methods. In the analytical part, challenges of 3d printed clay formwork using mobile robots are analysed in a geometrical and mathematical way regarding constraints from mobile robot, material properties and fabrication process. Next, the geometrical and mathematical questions are answered in the development of a parametric workflow for computational print path design. The parametric workflow was then evaluated on two demonstrator geometries: column and wall. In the experimental part, the feasibility of the development was evaluated by manufacturing the column in 1:1 scale.

The major challenges of designing 3D printed clay formwork using mobile robots lies in segmentation, stiffening and jointing. The segmentation is the general problem concerning in what way a large formwork can be segmented into smaller parts so that each part can be fit into the range of one mobile robot and in what sequence these segments can be built up into a whole. Special to clay formwork printing, the segmentation should also take the casting process into consideration, in which concrete will function as support for the formwork. The stiffening concerns how the formwork can be designed to be self-supporting to withstands its self-weight and the hydrostatic pressure from liquid concrete. The jointing problem concerns how jointing details between formwork tiles can be designed and integrated to achieve a stably interlocking between formwork tiles.

For the print path design the 3D modelling software Rhinoceros 7 with parametric modelling environment Grasshopper is used. The design process is developed parametrically with programming language Python. The computational development of print path design is written into grasshopper components that can be applied as a print path design tools for the generation of print path for user defined geometries.

The print path design tools are applied to two use cases: a column and a wall. The outcome of the application is two print path models, each of which consisting of sequences of spatial frames that describe the movement of robot end-effector and corresponding robot frames that describes the location of mobile robots.

In the experimental part, the column is fabricated in 1:1 scale to test the print path model and fabrication process. The clay formwork is printed with a Universal Robots UR10e robot arm

installed on a mobile platform. A fast-setting concrete is cast incrementally in the printing process to support the clay formwork.



Figure 5: Diagram of research method.

## 4.2. Segmentation

The segmentation of clay formwork is the general problem concerning in what way a large formwork can be segmented into smaller parts. The geometrical representation of a clay formwork is a 3-dimensional surface. The segmentation on the ground plane and the segmentation on the formwork surface deals with different concerns and restrictions. The segmentation on the ground plane is restricted by the range of mobile robots; the segmentation on the formwork surface concerns robot end-effector collision, and the casting process. So, the 3-dimensional problem of segmentation is considered on the ground plane and on the formwork surface separately.

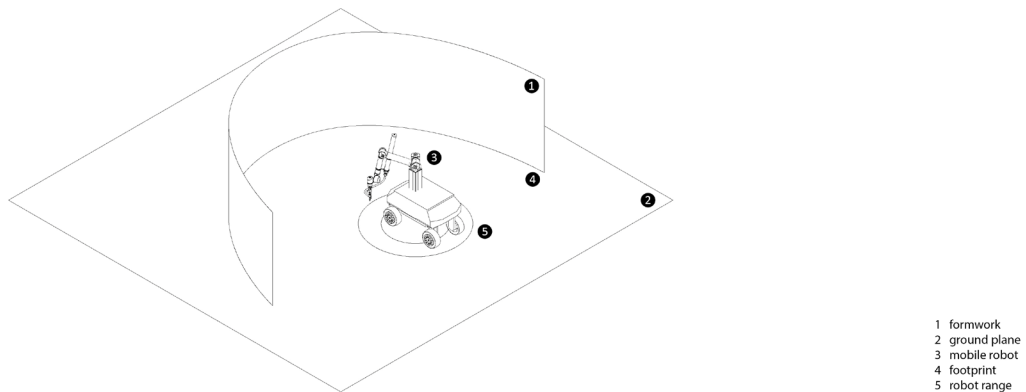


Figure 6: Illustration of terms for the segmentation.

For the segmentation on the ground plane, the major objective is to find the initial splitting points on the footprint of the formwork based on the range of mobile robots. The challenge of this step is to split the footprint of the formwork in a way that each segment of the footprint

stays within the range of one mobile robot and a minimal number of footprint segments are created. Looked from the fabrication side, the purpose of this step is to allow the mobile robot to print as large a segment as it can at one location, therefore minimizing the count of robot relocation that is needed to print out the whole formwork.

The footprint of formwork has a geometrical representation as a curve. The robot range can be geometrically represented with a pair of concentric circles. The outer range describes the farthest distance from the robot origin that the robot can reach; and the inner range describes the minimal distance from the robot origin it requires to avoid collision with the mobile platform.

For a footprint curve with a constant curvature (e.g., an arc or a line), the maximal segment length is a value relevant to the curve curvature and the robot range. This value can be either calculated algebraically or found with geometrical method, which is shown in the illustration below.

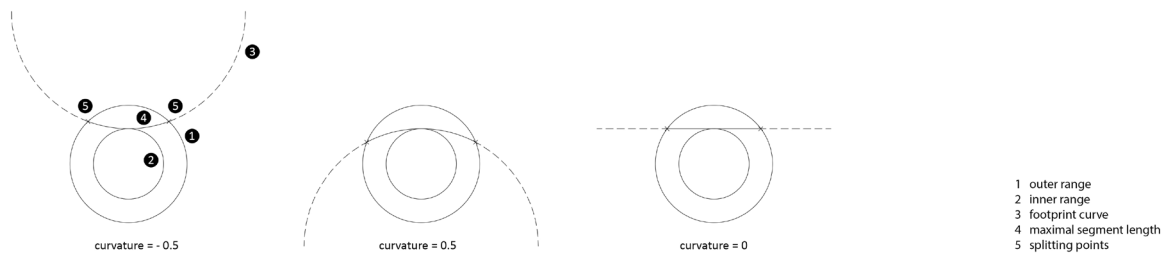


**Figure 7: Maximal segment length in relation to footprint curvature and robot range. In illustration, the outer range has a radius of 0.6 meter and the inner range has a radius of one meter.**

After the maximal segment length is found, the next step is to divide the footprint curve. The best way to do this in Grasshopper is to divide the footprint curve evenly using the “Divide Curve” component. The “Divide Curve” component asks for the footprint curve, the curve length which can be calculated with the “Length” component, and the division count which can be calculated by integer dividing the curve length by the maximal segment length.

For a footprint curve with variable curvatures, the method of dividing the footprint curve by a constant maximal segment length cannot be applied because the neither the curve curvature nor the maximal segment length is not a constant value. In this case, the initial splitting points are found with a geometrical method.

The input geometries are the footprint curve and the pair of concentric circles representing the robot range. The splitting points are found one after another. The first splitting point is

always the start point of the curve. Then I define the second splitting point as a variable that moves away from the first splitting point along the curve towards the end of the curve. I want to create a circle that passes through the first and second splitting points which has a radius of the outer robot range. Next, I can create a concentric circle with a radius of the inner robot range. As the second splitting point moves farther away from the first splitting point, the inner circle gets closer to the footprint curve. Once the inner circle is tangent to the footprint curve, the maximal segment length is achieved.

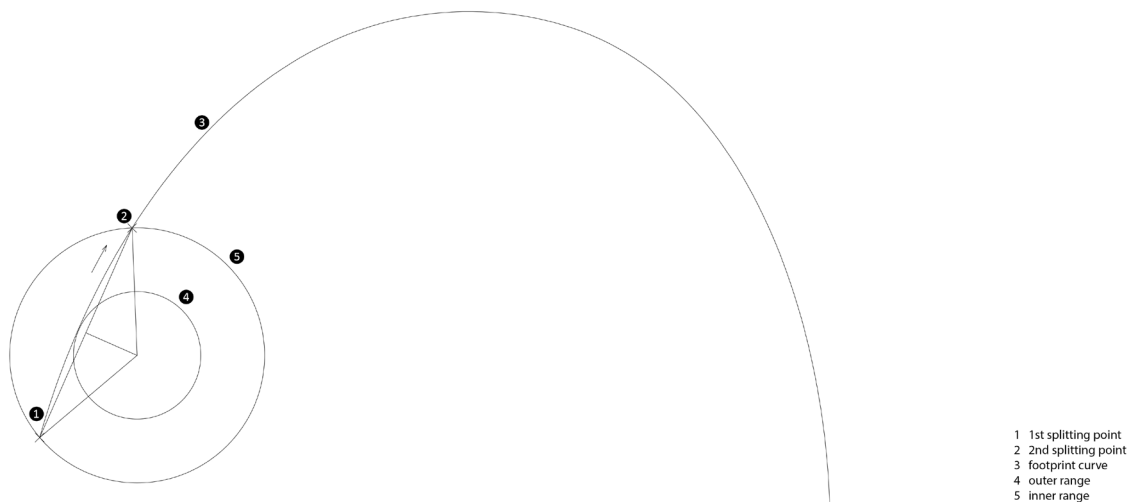


**Figure 8: First segment found with geometrical method on a footprint curve with variable curvature.**

After the second splitting point is found, it is recorded as a constant and the third splitting point is created as a variable that moves away from the second splitting point along the curve towards the end. A new pair of concentric circles are created in the same way using the second and the third splitting points and the same robot range. This process is repeated until last splitting point reaches the end point of the curve. Robot frames are also found in this process together with all the splitting points.

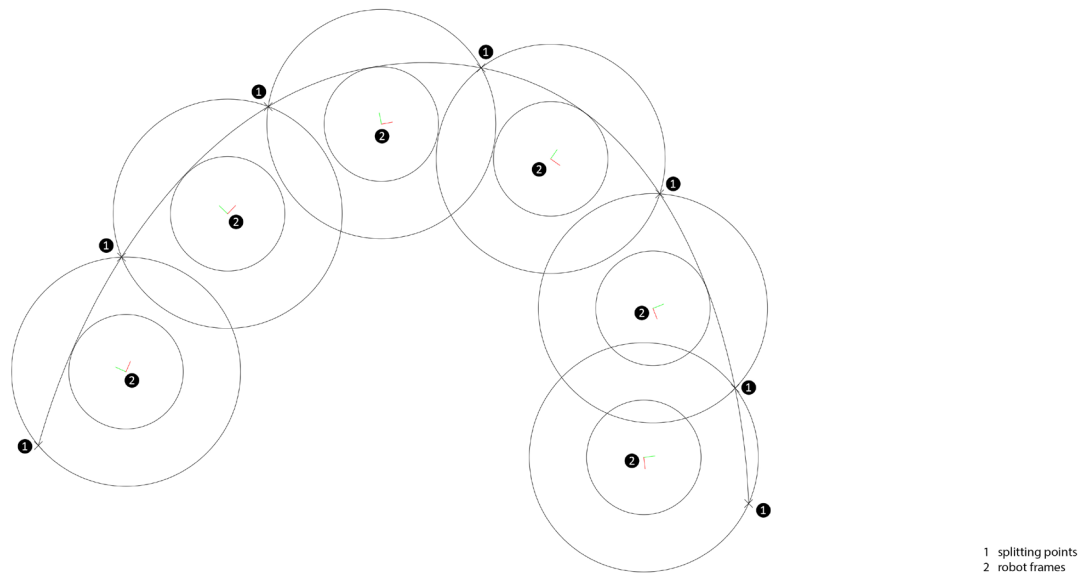


**Figure 9: Splitting points, robot ranges and robot positions found on a footprint curve with variable curvature.**

There is one problem with the result shown in the picture above: on the one hand, the last segment is not fully utilizing the robot range as the previous segments do; on the other hand, the robot range of previous segments are fully exploited, allowing no room for further geometrical transformation in vertical direction. To solve this problem, I introduced a tolerance parameter to the robot range. With the tolerance parameter introduced, the algorithm does not calculate the result with the actual robot range, but with the robot range modified with tolerance value. The introduction of tolerance provides a safer division result; and it allows the designer to use the tolerance parameter as a way of optimisation. For example, the designer can adjust the tolerance to achieve a result in which the robot range utilization of last segment is like that of the previous segments.

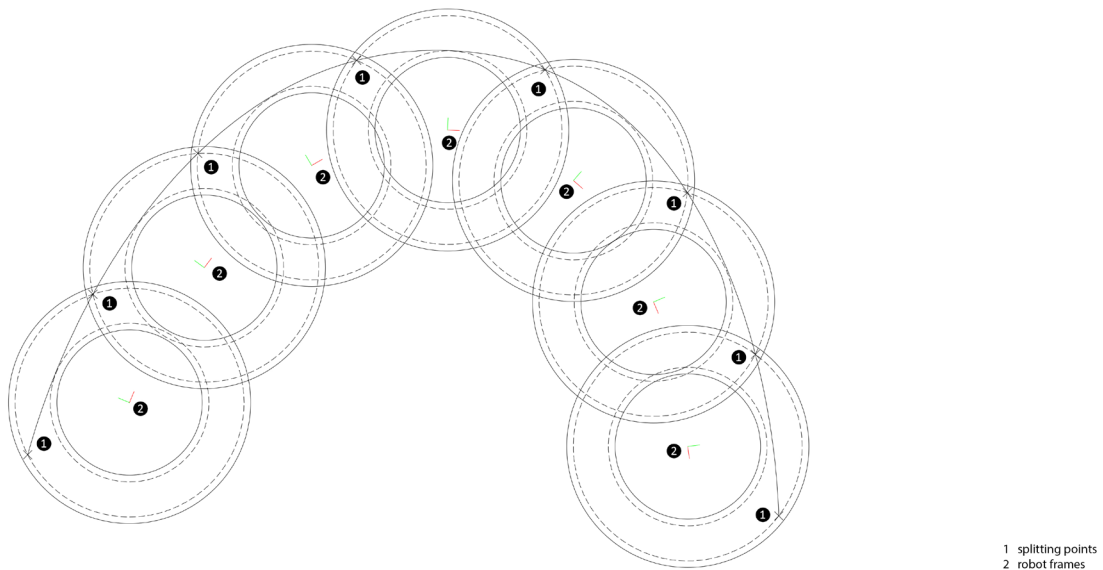


**Figure 10: Splitting points, robot ranges and robot positions found on a footprint curve with a tolerance parameter introduced.**

Both methods introduced above takes the robot range into consideration. Compared to the first division method which is based on a constant curve curvature, the second division method is also aware of the geometrical features of the footprint curve. The second method works with most input curves. However, in application, the formwork geometry could transform in vertical direction. Since this method only takes the footprint curve of the formwork surface into consideration, what this method creates is not an accurate calculation but a suggestion for the designer with visualised robot range and robot frames.

The next step is to look at the segmentation of formwork on the formwork surface. In this step, the geometries to begin with are the initial splitting points found in the previous step, the formwork surface, and layers of contour curves. The aim is to tessellate the formwork into tiles and split the contour curves of the formwork into curve segments and rearrange them into small groups that is related to the consecutive printing and casting process. To achieve this, I will firstly create a tessellation pattern, then split and group the contour curves accordingly.

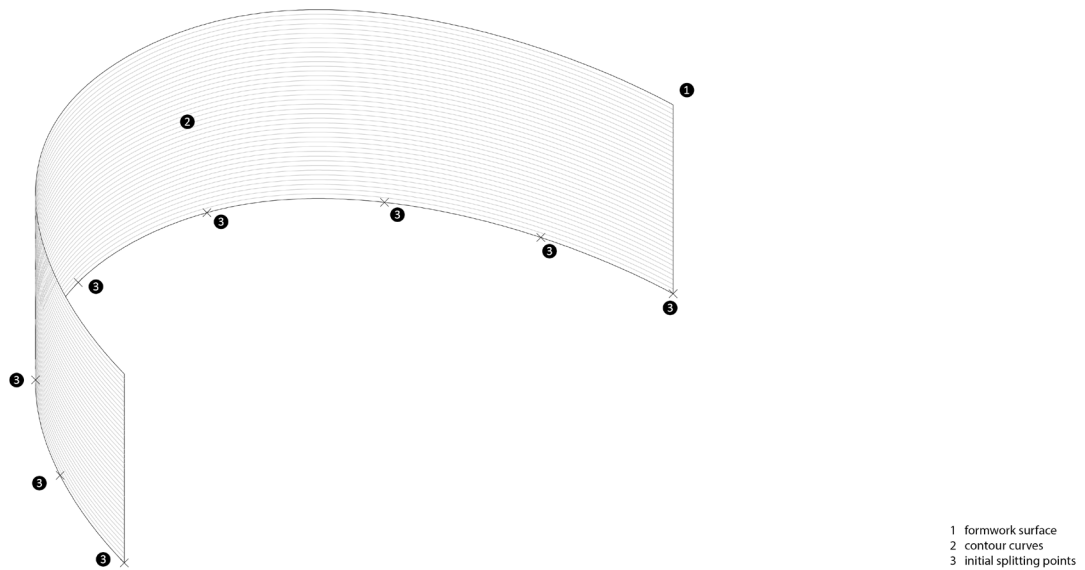


**Figure 11: Initial geometries for the segmentation on the formwork surface.**

To create a tessellation pattern on the formwork surface means to divide the whole surface into tiles. The restriction factors of the length, height and boundary of tiles are introduced below.

In the length direction, the tile is restricted by the robot range. The initial splitting points on the footprint indicate where the surface should be split. Each tile has a length that could be covered in the range of one mobile robot.

In the height direction, an incremental printing and casting process restricts how high a tile could be. In an incremental printing and casting process, concrete is cast in the intervals of formwork printing. In one cycle of this process, a row of clay formwork is printed to a certain height first, then a volume of fast-setting concrete is cast into the clay formwork to the height of clay formwork. This volume of concrete hardens very quickly and after it hardens, another cycle could begin. A new row of clay formwork is printed on top of the previous row, which is supported by the hardened concrete and a new volume of concrete is cast afterwards. The height increment of each cycle is the maximal height at which the clay formwork can withstand its self-weight and the hydrostatic pressure from liquid concrete. This height is used as the tile height.

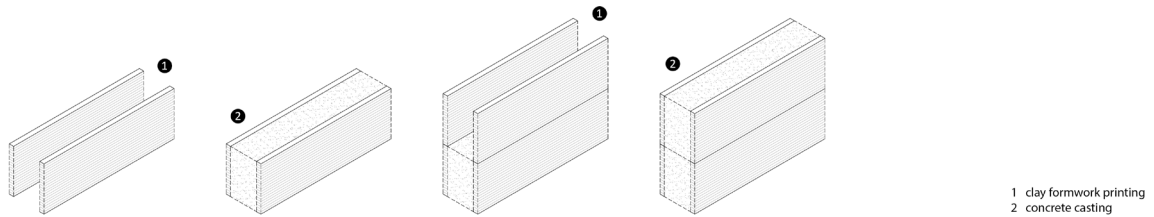


Figure 12: Diagram of a consecutive printing and casting process.

Another restriction in the fabrication process that must be considered is the end-effector collision. To avoid the robot end-effector colliding into other tiles of clay formwork during printing, there should be a minimal angle between the robot end-effector axis and the boundary between neighbouring tiles in one row. One option is to tilt the axis of end-effector. Another option is to design tilted boundaries between neighbouring tiles. This option allows the end-effector to work in a vertical axis without colliding into printed objects. The previous option requires a complex robot configuration, the latter option brings up challenges in print path modelling. In terms of effort, neither one has a big advantage over the other. However, my supervisor Guido Dielemans and I noticed in our experiment that when a tilted end-effector traverses over the printed clay formwork, it scratches and damages the print. In this thesis, the second option is adopted. The end-effector collision is avoided by tilting the tile boundaries.

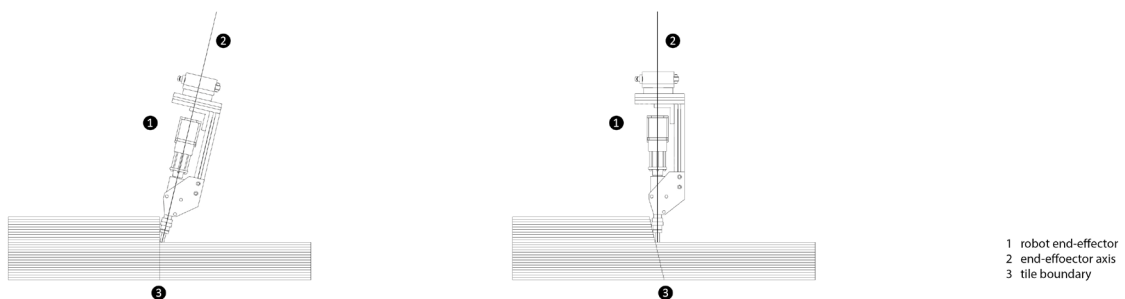
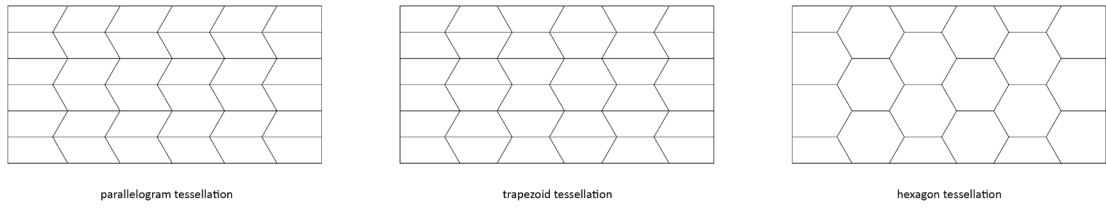


Figure 13: Two strategies to avoid the end-effector collision. Left: tilted end-effector axis. Right: tilted tile boundary.

Based on the tile length, tile height and tilting angle of the tile boundaries, tessellation strategies can be drawn out. It could either be a parallelogram, a trapezoid, or a hexagon tessellation, which is introduced by Guido.



**Figure 14: Tessellation strategies.**

Both parallelogram and trapezoid tessellation meets the above-described design requirements. However, the trapezoid tessellation has a big advantage over the parallelogram tessellation. If we look at one row of tiles, the tiles in a parallelogram tessellation can only be built one after another. This only allows for a lineal fabrication sequence. While in a trapezoid tessellation, tiles do not need to be fabricated in a lineal order. This feature allows for the possibility of using multiple robots to realise a cooperative fabrication.

The hexagon tessellation is based on the same geometrical grid of a trapezoid tessellation but has advantages. First, the rows of tiles in a hexagon tessellation interlock with each other, which increases the stability of the formwork. Second, a hexagon tessellation requires much fewer numbers of robot relocation.

The hexagon tessellation is chosen to be applied to the formwork surface in this thesis because of its advantages over the other two. Prior to segmentation, a primitive print path model of the whole clay formwork is created by slicing the formwork surface with horizontal planes into layers. The print path model in this stage is a list of contour curves. Next, the contour curves will be split and regrouped according to the hexagon tessellation.

For the first contour curve, a list of points on the curve is found by using the grasshopper component “Curve Closest Point”. The source points are the initial splitting points. Then, the splitting points are found by shifting these points on the curve by a distance  $shift_{initial}$ . If the index of point  $index_{point}$  is even, the initial shift distance is a positive value, which means that the point is moved in curve direction. If the index of point is odd, the initial shift distance is a negative value, which means that the point is moved backwards to curve direction. At last, the contour curve is split into segments using the grasshopper component “Shatter” with the splitting points. The tile height and the boundary tilt angle are noted as  $h_{tile}$  and  $\theta_{boundary}$ .

$$shift_{initial} = \frac{h_{tile} \cdot \tan(\theta_{boundary})}{2} \cdot direction_{point}$$

$$direction_{point} = \begin{cases} 1, & index_{point} \in 2\mathbb{N} \\ -1, & index_{point} \in 2\mathbb{N} + 1 \end{cases}$$

From the second contour curve, a list of point on the curve is found using “Curve Closest Point”, the source points being the splitting points on the previous contour curve. Then, the splitting points are found by moving these points on the curve by a distance *shift*. Same as for the first contour curve, points with even and odd index are moved in opposite directions. In addition, the direction of movement is reversed every tile. The layer index is noted as *index<sub>layer</sub>*. Value *m* in the equation below indicates the layer count per tile, which is the tile height divided by layer height. Finally, the contour curve is split into segments using “Shatter” with the splitting points.

$$shift = -h_{layer} \cdot \tan(\theta_{boundary}) \cdot direction_{point} \cdot direction_{layer}$$

$$direction_{point} = \begin{cases} 1, & index_{point} \in 2\mathbb{N} \\ -1, & index_{point} \in 2\mathbb{N} + 1 \end{cases}$$

$$direction_{layer} = \begin{cases} 1, & 0 \leq index_{layer} \% 2m < m \\ -1, & m \leq index_{layer} \% 2m < 2m \end{cases}$$

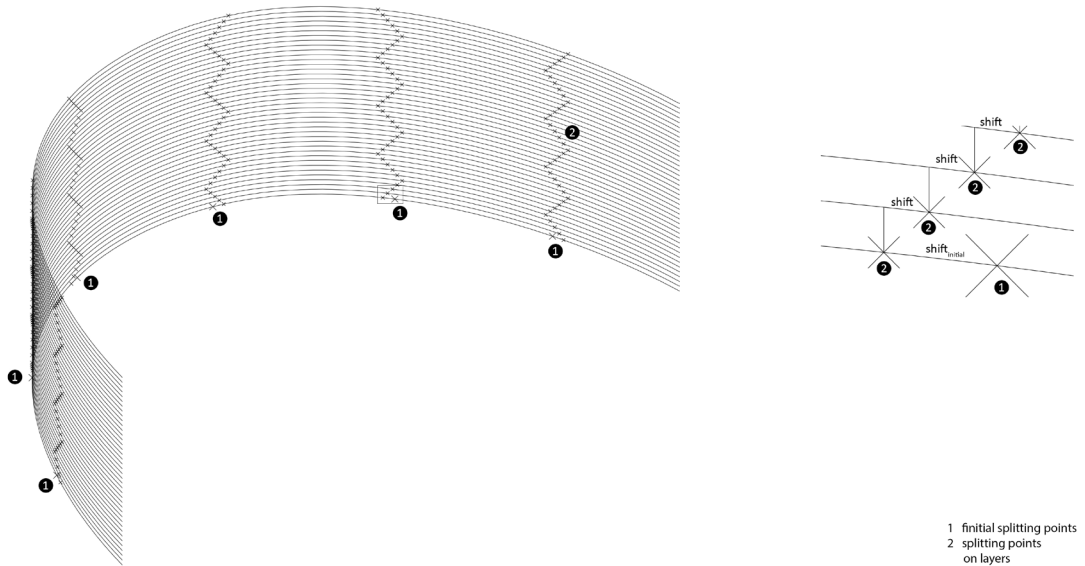


Figure 15: Splitting points found on layers of contour curves.

All the shattered contour curve segments are stored in one single list. The data structure of the segments is illustrated below in which *n* is the count of segments per layer.

$$\begin{array}{ccccccc}
 \dots & \dots & \dots & \dots & \dots & \dots & \dots \\
 n & n+1 & n+2 & n+3 & \dots & 2n-2 & 2n-1 \\
 0 & 1 & 2 & 3 & \dots & n-2 & n-1
 \end{array}$$

Next, for each segment, a tile index and a segment key are calculated from its segment index. The tile index describes which tile this segment belongs to; and the segment key indicates the layer index of this segment in its corresponding tile. The following data structure should be the outcome. This table describes the situation when the segment count per layer  $n$  is an even number. Again, the layer count per tile is noted as  $m$ . Each half hexagon tile has a layer count of  $m$ ; and each full hexagon tile has a layer count of  $2m$ .

...	...	...	...	...	...	...	...
	$n, m+1$	$\frac{3n}{2}, 1$	$n+1, m+1$	$\frac{3n}{2}+1, 1$	...	$\frac{3n}{2}-1, m+1$	$2n-1, 1$
	$n, m$	$\frac{3n}{2}, 0$	$n+1, m$	$\frac{3n}{2}+1, 0$	...	$\frac{3n}{2}-1, m$	$2n-1, 0$
$v=1$	$n, m-1$	$\frac{n}{2}, 2m-1$	$n+1, m-1$	$\frac{n}{2}+1, 2m-1$	...	$\frac{3n}{2}-1, m-1$	$n-1, 2m-1$
	...	...	...	...	...	...	...
	$n, 1$	$\frac{n}{2}, m+1$	$n+1, 1$	$\frac{n}{2}+1, m+1$	...	$\frac{3n}{2}-1, 1$	$n-1, m+1$
	$n, 0$	$\frac{n}{2}, m$	$n+1, 0$	$\frac{n}{2}+1, m$	...	$\frac{3n}{2}-1, 0$	$n-1, m$
	$0, m-1$	$\frac{n}{2}, m-1$	$1, m-1$	$\frac{n}{2}+1, m-1$	...	$\frac{n}{2}-1, m-1$	$n-1, m-1$
	...	...	...	...	...	...	...
$v=0$	$0, 1$	$\frac{n}{2}, 1$	$1, 1$	$\frac{n}{2}+1, 1$	...	$\frac{n}{2}-1, 1$	$n-1, 1$
	$0, 0$	$\frac{n}{2}, 0$	$1, 0$	$\frac{n}{2}+1, 0$	...	$\frac{n}{2}-1, 0$	$n-1, 0$
	$u=0$	$u=1$	$u=2$	$u=3$	...	$u=n-2$	$u=n-1$

To achieve the new data structure, the following values are calculated for each segment. Value  $u$  indicates the horizontal position of the segment in the tessellation. Value  $v$  indicates the vertical position of the segment's corresponding tile.

$$u = index_{segment} \% n$$

$$index_{layer} = bottom\left(\frac{index_{segment}}{n}\right)$$

$$v = \begin{cases} bottom\left(\frac{index_{layer} + m}{2m}\right), & u \in 2\mathbb{N} \\ bottom\left(\frac{index_{layer}}{2m}\right), & u \in 2\mathbb{N} + 1 \end{cases}$$

With the  $u$  and  $v$  values, the tile index  $index_{tile}$  and the segment key  $key$  can be calculated.

$$index_{tile} = \begin{cases} v \cdot n + \frac{u}{2}, & u \in 2\mathbb{N} \\ v \cdot n + \frac{n}{2} + \frac{u-1}{2}, & u \in 2\mathbb{N} + 1 \end{cases}$$

$$key = \begin{cases} index_{layer} - (2v - 1) \cdot m, & u \in 2\mathbb{N} \\ index_{layer} - 2v \cdot m, & u \in 2\mathbb{N} + 1 \end{cases}$$

In this way, from each segment index the tile index and segment key can be calculated. Reversely, from a tile index and a segment key, the corresponding segment can be found.

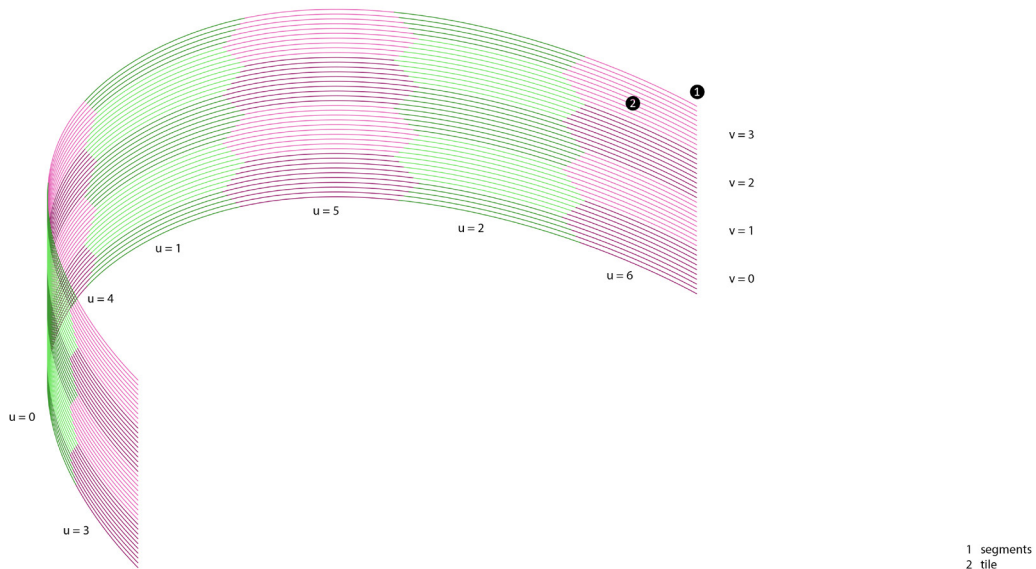


Figure 16: Segmented contour curve regrouped into tiles according to the tessellation.

The outcome of the whole segmentation process is a “Tessellation” Python class object. In a “Tessellation” object, tiles are stored as subclass object “Tile” with properties such as u value and v value; and contour curve segments are stored as subclass object “Segments” with properties such as tile index and segment key. The segment count per layer n, the layer count per tile m and geometrical parameters like layer height and tilt angle are stored as properties of “Tessellation”

### 4.3. Stiffening

The printed clay formwork is very fragile and soft and usually they rely on drying or sintering to achieve the necessary mechanical properties (Jipa and Dillenburger 2021). As clay has a large shrinkage percent while drying, the concrete must be cast when clay is still moisture to ensure geometrical accuracy. Sintering is not an option because it removes clay formwork’s recyclability. The introduction of the incremental printing and casting process turned concrete into a supporting structure, reducing the requirement of structural strength of clay formwork. Still, more stiffening features must be integrated to the formwork print path to stabilize itself during printing and to withstand the hydrostatic pressure from liquid concrete during casting.

The first feature is undulation. This feature is introduced by Gido. By applying a sine-like undulation feature to the print path, the thickness of the clay formwork can be increased. The normal thickness of the clay formwork is dependent to the size of the print head. The thickness after application of undulation can be designed by adjusting the undulation amplitude.

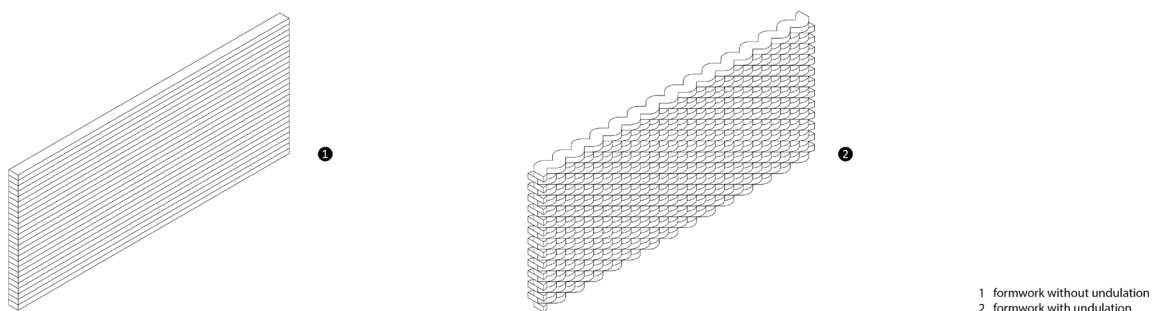


Figure 17: Model of clay formwork before and after application of undulation.

In the segmentation process introduced in the previous chapter, the intermediate outcomes include a list of contour curves and the splitting points on each contour curve. These

geometries will be used to apply the undulation feature. In addition, the length and amplitude of undulation  $length_{undulation}$  and  $amplitude_{undulation}$  must be defined.

To create the print path with undulation, the following computational method is used. For each layer, a list of division points and their corresponding curve tangent vectors are found using the grasshopper component “Divide Curve”. The division count is calculated with the curve length and the undulation length.

$$count = 4 \cdot \text{ceil} \left( \frac{length_{curve}}{length_{undulation}} \right)$$

For each division point  $Pt_{division}$ , its index in the division points list  $index_{point}$  and its perpendicular vector  $\vec{v}_{perp}$ , a interpolate point  $Pt_{interpolate}$  is found. The layer index is used here to flip the direction of undulation between adjacent layers. All the interpolate points calculated from one contour curve are put into a list. Then, an undulating curve is created from these interpolate points using the grasshopper component “Interpolate.”

$$direction_{layer} = \begin{cases} 1, & index_{layer} \in 2\mathbb{N} \\ -1, & index_{layer} \in 2\mathbb{N} + 1 \end{cases}$$

$$Pt_{interpolate} = \begin{cases} Pt_{division}, & index_{point} \in 4\mathbb{N} \\ Pt_{division} + direction_{layer} \cdot amplitude_{undulation} \cdot \vec{v}_{perp}, & index_{point} \in 4\mathbb{N} + 1 \\ Pt_{division}, & index_{point} \in 4\mathbb{N} + 2 \\ Pt_{division} - direction_{layer} \cdot amplitude_{undulation} \cdot \vec{v}_{perp}, & index_{point} \in 4\mathbb{N} + 3 \end{cases}$$

Then, the undulating curve must be split into segments. For each splitting point on the contour curve, a perpendicular frame is created, and a cutter object is created on each perpendicular frame. Splitting points on the undulating curve are found by calculating the intersection points between the undulating curve and the cutters. Next, the undulating curve is split into undulating segments with the splitting points on it using the “shatter” component.

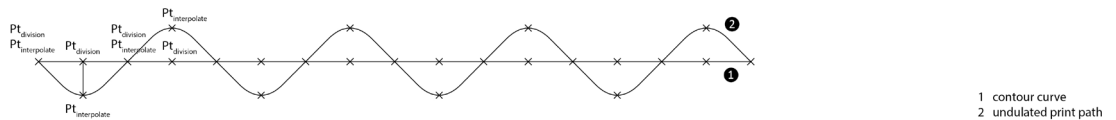
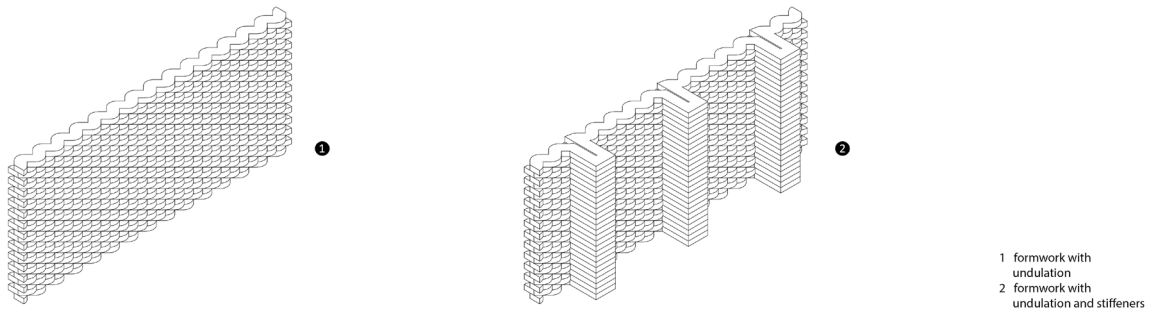


Figure 18: Print path before and after application of undulation.

To ensure that the list of undulating segments has the identical order to the list of contour curve segments, the undulating segments are sorted using Python list sorting function with the distance from the start point of undulating segment to the start point of splitting point as sort key. All undulating segments are put in a list with the identical order to the list of contour curves.

The second feature are the integrated stiffeners. The clay formwork is still not strong enough against the hydrostatic pressure after applying undulation. The stiffeners are vertical rib-like structures on the outer surface of clay formwork designed to work against the hydrostatic pressure. They are distributed horizontally along the formwork surface and each of them goes from the top to the bottom of the formwork. They are integrated into the clay formwork as a part of it. The following section describes the method I used to integrate them into the print path design.



**Figure 19: Model of clay formwork before and after integration of stiffeners.**

On each layer, the first step is to find the inserting points. For the top layer, the initial inserting points are found by dividing a contour curve segment using a given stiffening distance. For the rest of the layers, the inserting points are the closest points on the current layer from the inserting points on the previous layer. This point finding method is to ensure that the stiffener traverse on a shortest path from the top to the bottom of the formwork. Then, a vector describing the length and direction of the stiffener is calculated for each inserting point. The direction of the stiffener vector is the direction perpendicular to the contour curve. The method to calculate the stiffener length is described in detail below.

The lengths of stiffeners are calculated with the aim of preventing the formwork from tipping over during printing and casting. To do that, I created the following physical model to find the relation between the tilt angle of formwork and the required stiffener length. The model is a rectangular formwork tile supported by one stiffener. The tile has the length of the previously given stiffening distance, the layer count and the height of a full hexagon. Additional values include the width and height of a layer of clay, the density of clay, the density of concrete and the undulated length factor which is the length of undulated curve divided by the corresponding contour curve.

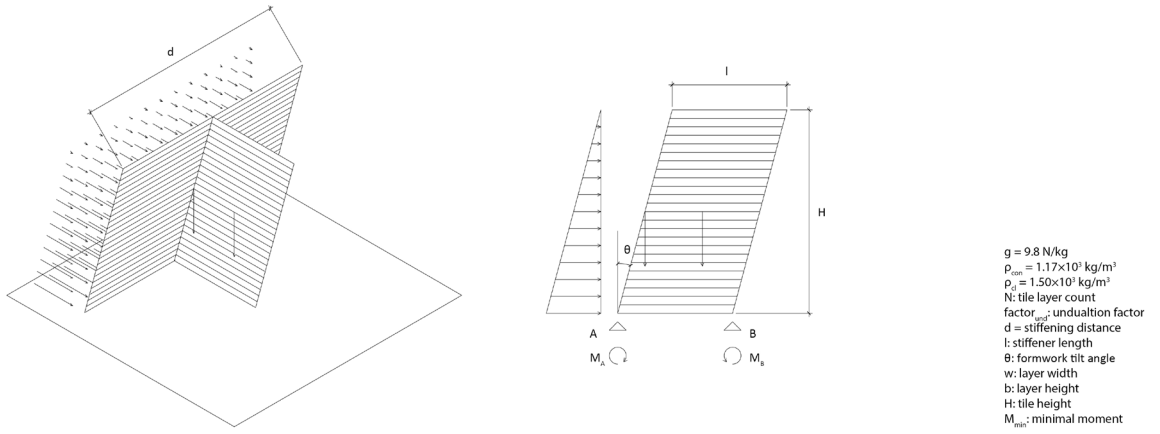


Figure 20: Physical model to calculate the stiffener length from the formwork tilt angle.

Clockwise to support point  $B$ , the moment from hydrostatic pressure, self-weight of formwork and self-weight of stiffener are noted as  $M_{hp,B}$ ,  $M_{f,B}$  and  $M_{s,B}$ . The moment of the support reaction  $A$  is noted as  $M_A$ . A given minimum moment is noted as  $M_{min}$ . The following condition is set to prevent the formwork from tipping over.

$$\begin{cases} M_{hp,B} + M_{f,B} + M_{s,B} + M_A = 0 \\ M_A > M_{min} \end{cases}$$

$$M_{hp,B} = \int_0^H \frac{\rho_{con} \cdot g \cdot d \cdot h^2}{\cos \theta} dh$$

$$M_{f,B} = N \cdot factor_{und} \cdot d \cdot w \cdot b \cdot \rho_{cl} \cdot g \cdot \left( \frac{H \cdot \tan \theta}{2} - l \right)$$

$$M_{s,B} = N \cdot 2 \cdot l \cdot w \cdot b \cdot \rho_{cl} \cdot g \cdot \left( \frac{H \cdot \tan \theta}{2} - \frac{l}{2} \right)$$

Anti-clockwise to support point  $A$ , the moment from hydrostatic pressure, self-weight of formwork and self-weight of stiffener are noted as  $M_{hp,A}$ ,  $M_{f,A}$  and  $M_{s,A}$ . The moment of the support reaction  $B$  is noted as  $M_B$ . Likewise, the following condition is set.

$$\begin{cases} M_{hp,A} + M_{f,A} + M_{s,A} + M_B = 0 \\ M_B > M_{min} \end{cases}$$

$$M_{hp,A} = - \int_0^H \frac{\rho_{con} \cdot g \cdot d \cdot h^2}{\cos \theta} dh$$

$$M_{f,A} = -N \cdot factor_{und} \cdot d \cdot w \cdot b \cdot \rho_{cl} \cdot g \cdot \frac{H \cdot \tan \theta}{2}$$

$$M_{s,A} = -N \cdot 2 \cdot l \cdot w \cdot b \cdot \rho_{cl} \cdot g \cdot \left( \frac{H \cdot \tan \theta}{2} + \frac{l}{2} \right)$$

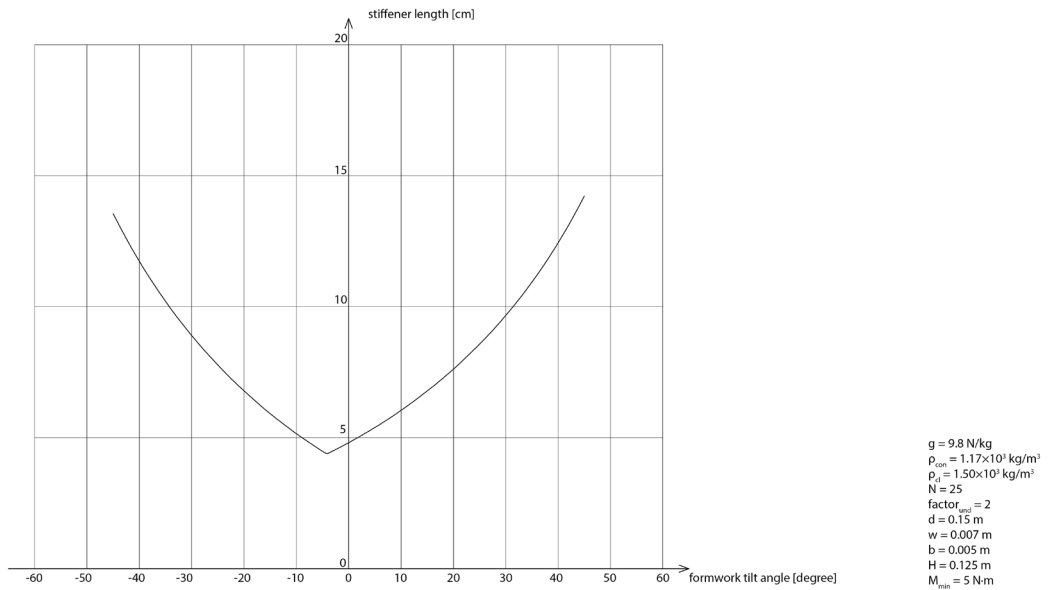


**Figure 21: Relation between the formwork tilt angle and the stiffener length required to avoid tipping over. The parameters used are listed next to the graph.**

Back to the creation of stiffeners, on each layer and local to each inserting point, a local tilt angle  $\theta$  can be calculated from the layer height and the distance between current inserting point and the corresponding inserting point on the previous layer (the next layer in case of the top layer). Then, the length of stiffener can be calculated using the method introduced above.

$$\theta = \cos^{-1} \left( \frac{height_{layer}}{distance_{current,previous}} \right)$$

Next, stiffener polylines are created and inserted into the print path. For each stiffener vector, a series of points are drawn based on it. A polyline is created from these points. Two intersection points are found using a curve-to-curve intersection tool. The polyline and the path are both shattered with the intersection points. Unwanted curve segments are culled, and the remaining curves are joined into one continuous path. The following figure shows an example of stiffener polyline created from the stiffener vector.

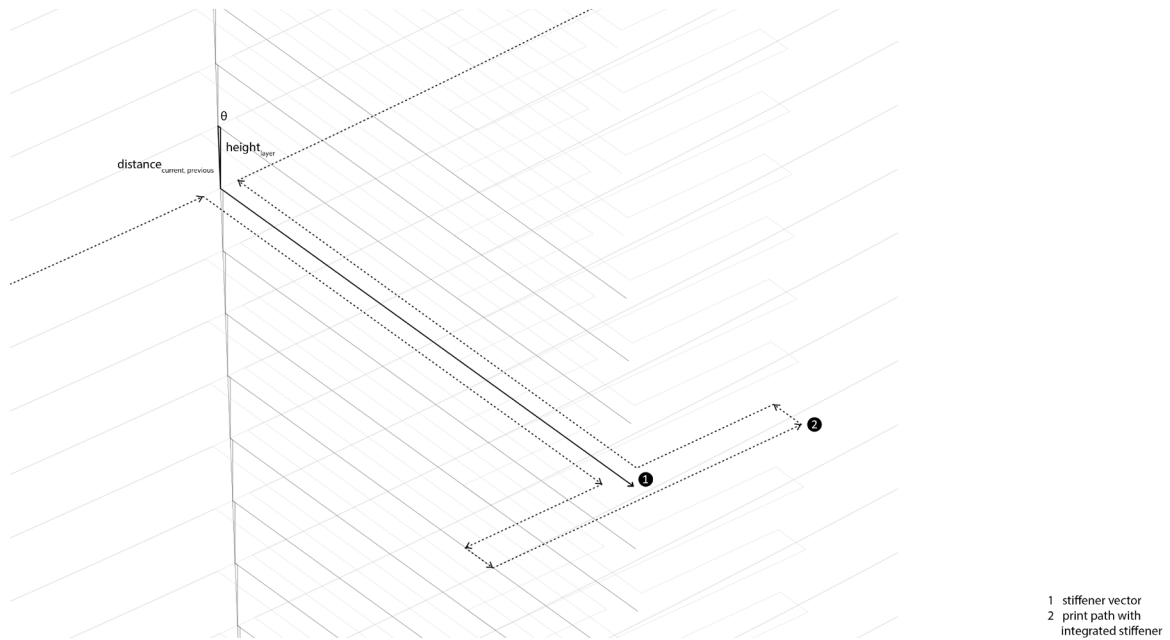


Figure 22: Stiffener polyline created from the stiffener vector and integrated into the print path.

#### 4.4. Jointing

The jointing feature is designed to ensure a stable interlocking between clay formwork tiles. An extended surface is added to the vertical boundaries of each tile. This extended surface increases the contact area between tiles. However, the boundary tilt angle usually requires more than 30 degrees, which is much larger than the maximal allowable overhang angle in clay printing. The extended surfaces could not support themselves during printing. A supporting volume is added underneath the extended surface. The supporting volume has on the other side the maximal overhang angle. Both the extended surface and the supporting volume are created in the clay printing process. Like the stiffeners, the jointing detail is created by integrating joint polylines into the print path.

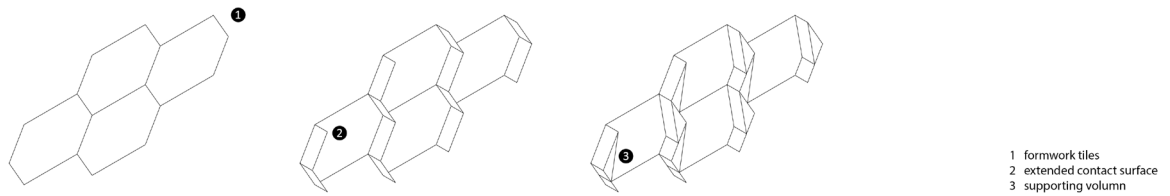


Figure 23: Concept of jointing.

The joint polylines integrated the print paths are designed as shown in the picture below. Before joints are integrated, the print path is simply split up with a point. The contact area between tiles is thus too small. Also, the width of the print path is not considered so the robot end-effector collides into the ends of neighbouring segment during printing. After the integration of joints, the contact area is increased. And a gap is created between neighbouring segments to tolerate the width of the print path.

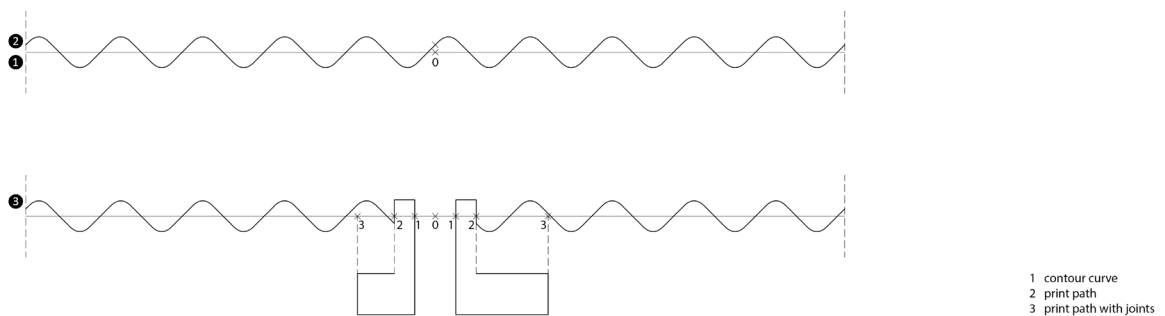


Figure 24: Print path before and after the integration of joints.

To parametrically model the joint polylines, three locations are found on both ends of each contour curve segment. Location one indicates the location of the extended surface. It is

found by shifting the end points towards inside by half path width so that neighbouring segments just touch each other. Location two indicates where to split the undulated print path and where the joint polyline ends. It is found by shifting location one towards inside by half path width. Location three is found regarding the maximal overhang angle of clay printing. On the top layer of each tile, location three is found by shifting location two towards inside by half path width. On the rest of the layers, it is found by shifting the closest point on the contour curve from location three on the previous layer towards outside by a distance allowed by the maximal overhang angle but no further than location two shifted towards inside by half path width.

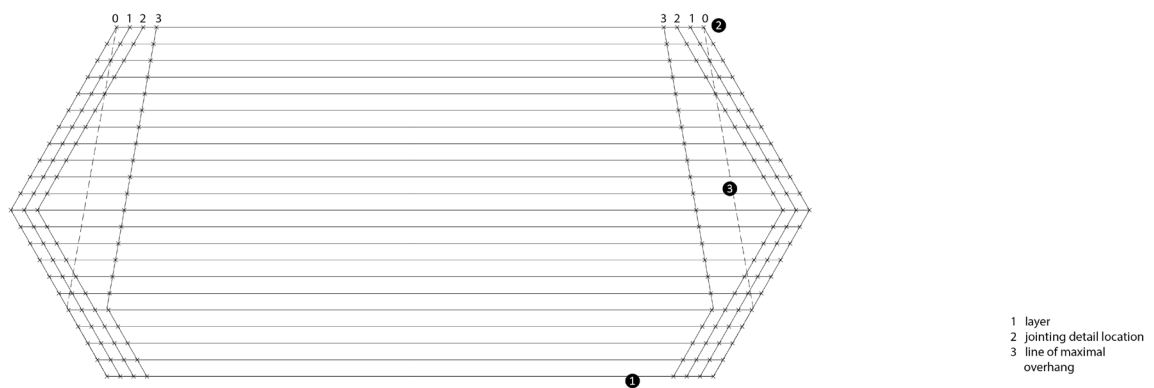


Figure 25: Locations for jointing details on a tile.

After finding the locations for jointing detail, sub-curves are extracted from the contour curve. Sub-curve 1-2 is offset towards inside by the undulation amplitude. Sub-curve 2-3 is offset towards outside by the undulation amplitude plus the print path width. Sub-curve 1-3 is offset towards outside by the undulation amplitude plus two times the print path width. The undulated print path is split at location two and connected with the sub-curves to create a continuous print path. There are sharp connections between joint polylines and undulated print paths. An example of sharp connection is at the location two on the left side in figure 27. With the help from Julian Trummer, an algorithm is developed to avoid sharp connections between joint polylines and undulated print paths.

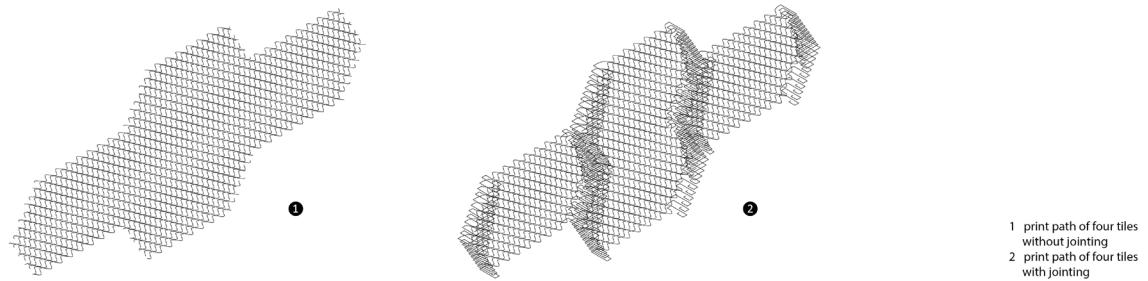


Figure 26: The print path of four tiles with and without integrated joints.

## 5. Results

The segmentation, stiffening and jointing methods are developed as a parametric workflow. User-defined geometries and parameters can be input into the workflow and a print path model is generated. To assess this parametric workflow, two demonstrator geometries are used to generate the print path model: column and wall. To evaluate the feasibility of the print path design in physical world, the column is experimentally fabricated in 1:1 scale.

### 5.1. Case 1: Column

The first use case of the parametric workflow is a column. The column geometry is designed by Gido. On the ground plane, it is a 3-way branching shaped constructed with six arc segments. In the vertical direction, it flows along a sine-curve. The column has a height of two metres and 400 layers in total with a layer height of 5 millimetres.

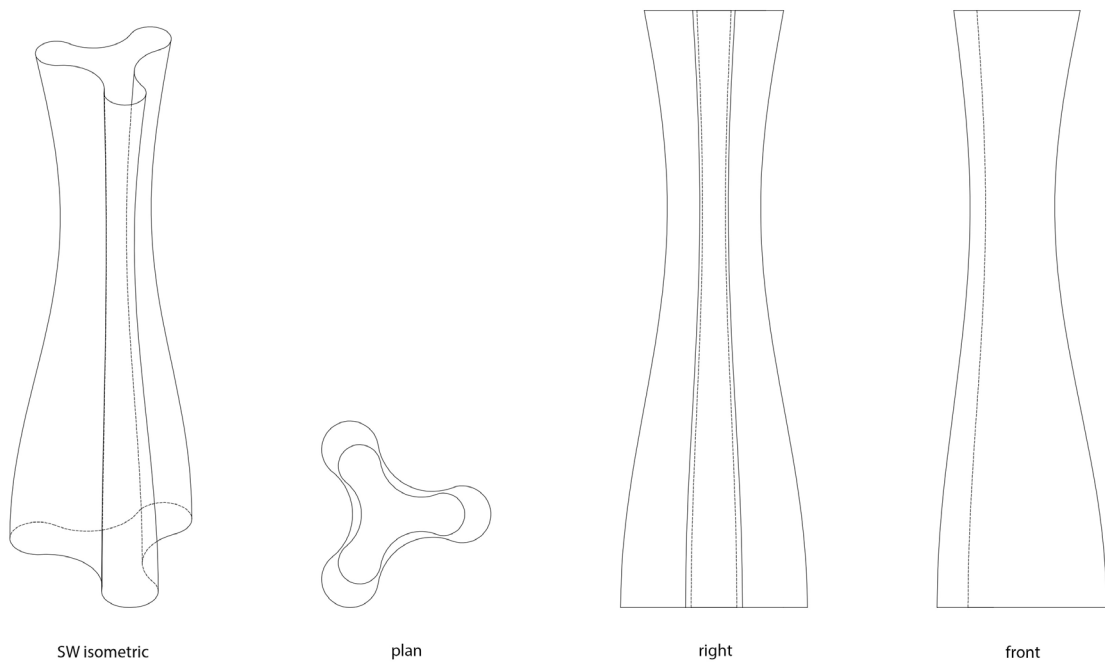


**Figure 27: Geometry of the demonstrator column.**

A hexagon tessellation pattern is applied to the formwork surface. On the ground plane, the footprint is split into six segments. A tile height of 25 layers, corresponding 12.5 cm is set for the segmentation on the formwork surface. The boundary tilting angle is set as 45 degrees. The result is a tessellation of 51 tiles, including 6 half hexagons and 45 full hexagons.

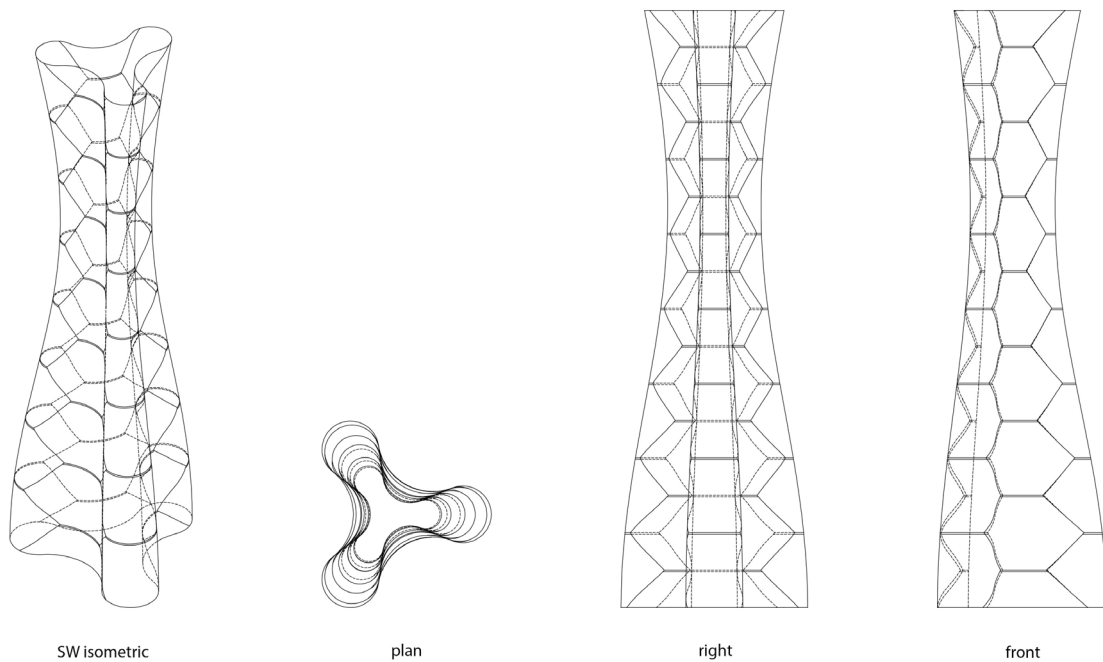


**Figure 28: Hexagon tessellation applied to formwork surface of the column.**

The contour curves on each layer are split into segments and grouped into tiles. 400 contour curves are segmented into 2400 segments. In the following pictures, I use different colours to illustrate different tiles.

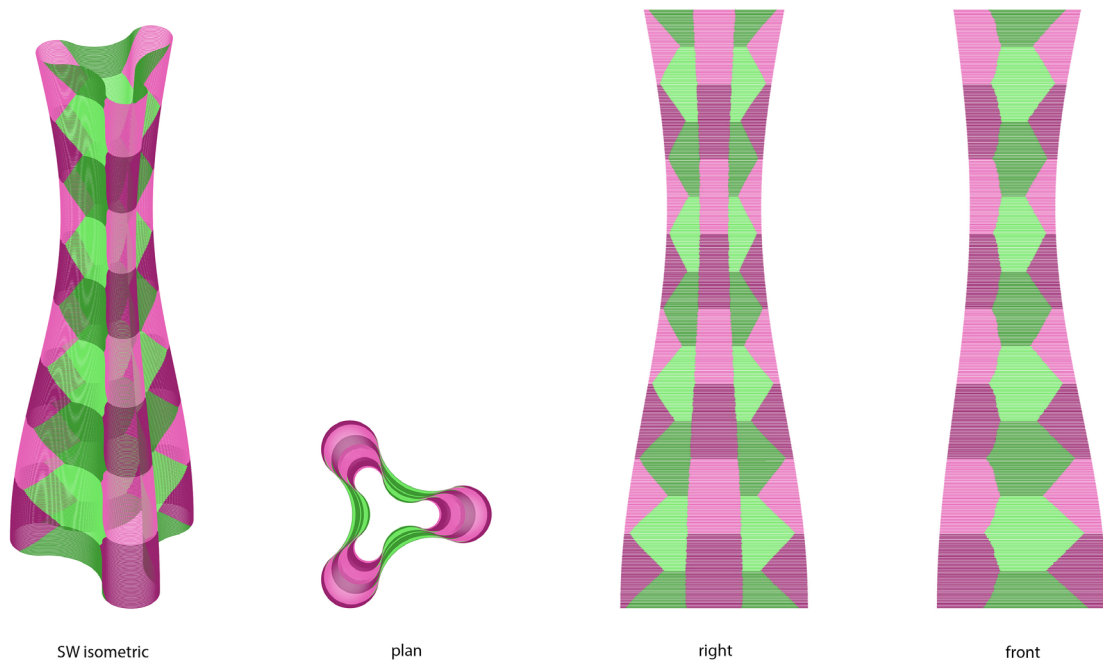


**Figure 29: Print path model of the column after segmentation.**

After segmentation, an undulation is applied to each layer. An undulation length of 16 mm and undulation amplitude of 6 mm is applied here. By applying undulation, the thickness of clay formwork is increased from 7mm, which is the diameter of the extruder tip, to 25 mm.

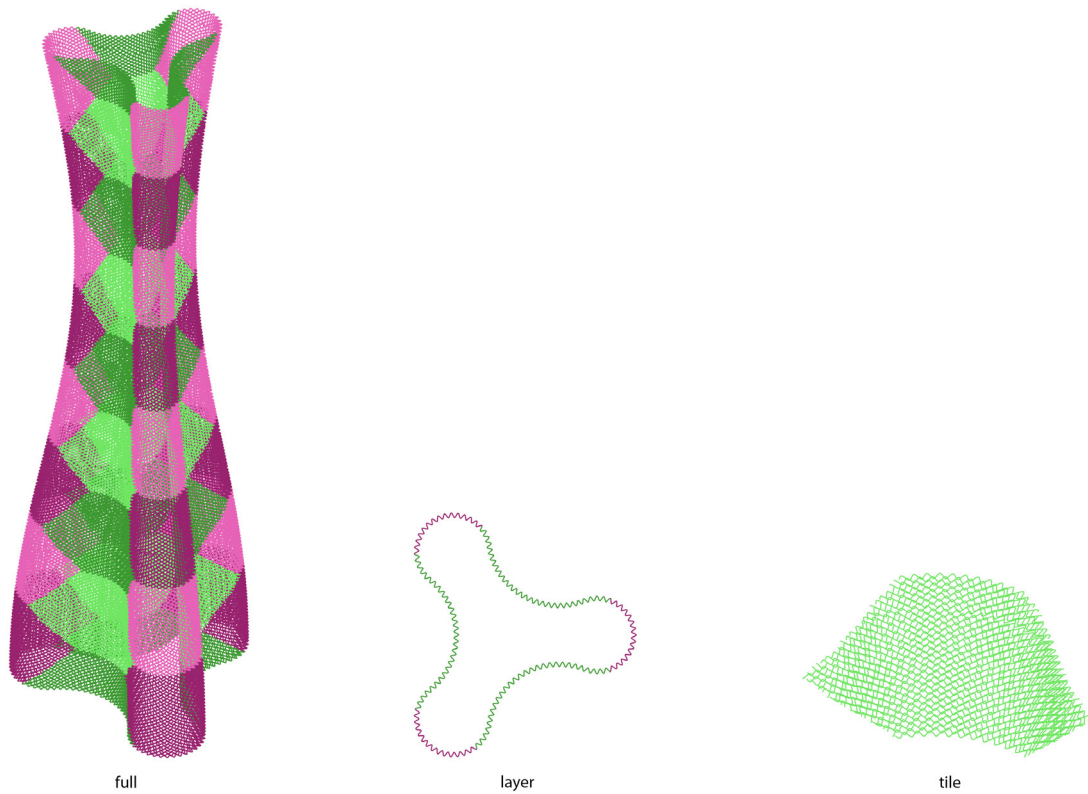


**Figure 30: Print path model of the column after integrating undulation.**

Six vertical stiffeners are integrated to the print path model. By the time of this use case, the method of calculating the length of stiffeners in relation to formwork tilt angle are still not developed. A uniform stiffener length of 6 cm is used here. The stiffeners polylines are designed as a spike-like shape. In the aim of reducing the mark on the inner surface of clay formwork, a cross connection is used to join the stiffener polylines and the print paths.

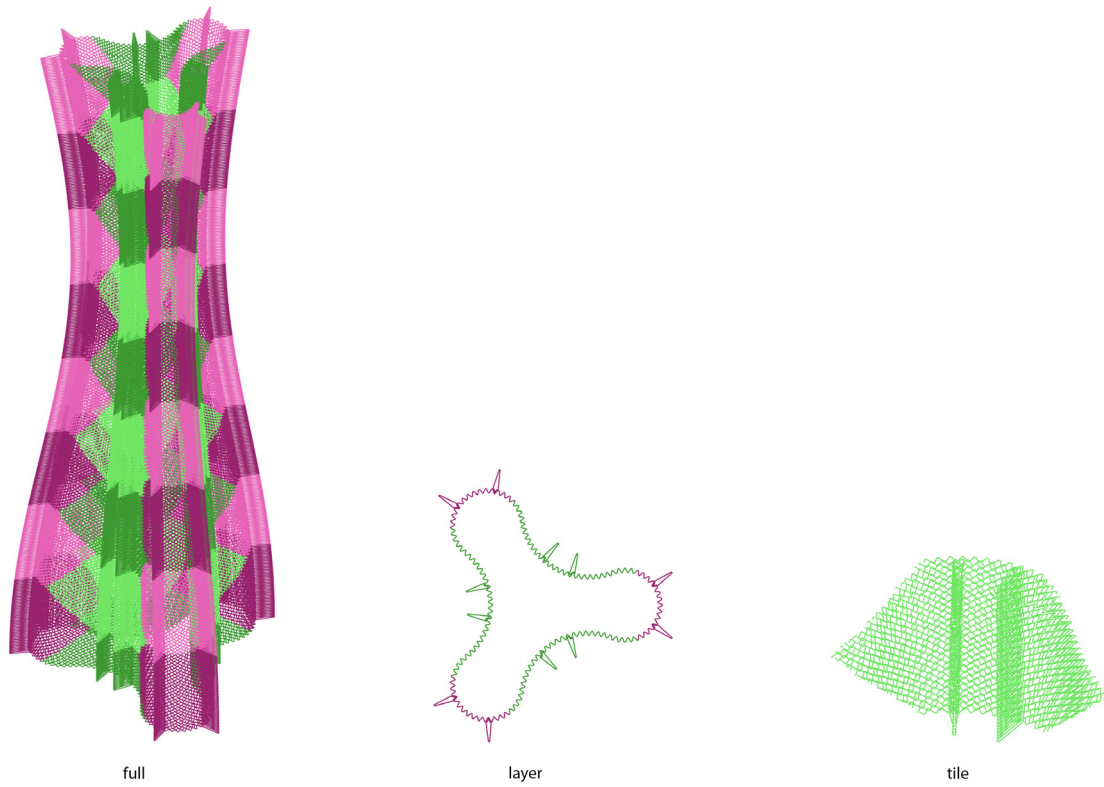


**Figure 31: Print path model of the wall after integrating stiffeners.**

At last, the end joints are integrated into the print path. A maximal overhang angle of 15 degrees is set here.

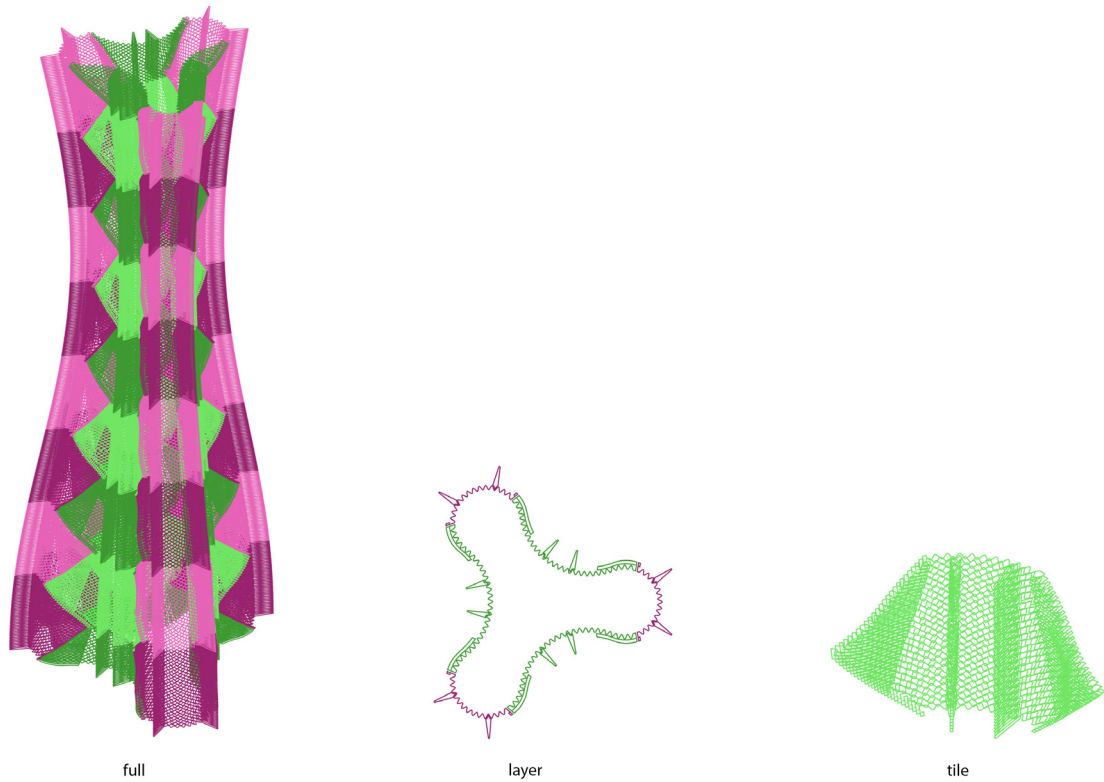


**Figure 32: Final Print path model of the column after integrating joints.**

## 5.2. Case 2: Wall

The second use case of the parametric workflow is a wall. On the ground plane, it has the shape of a half oval. In the vertical direction, the surface flows along a Bezier curve. Same as the use case of column, the wall has a height of two metres and 400 layers in total with a layer height of 5 millimetres.

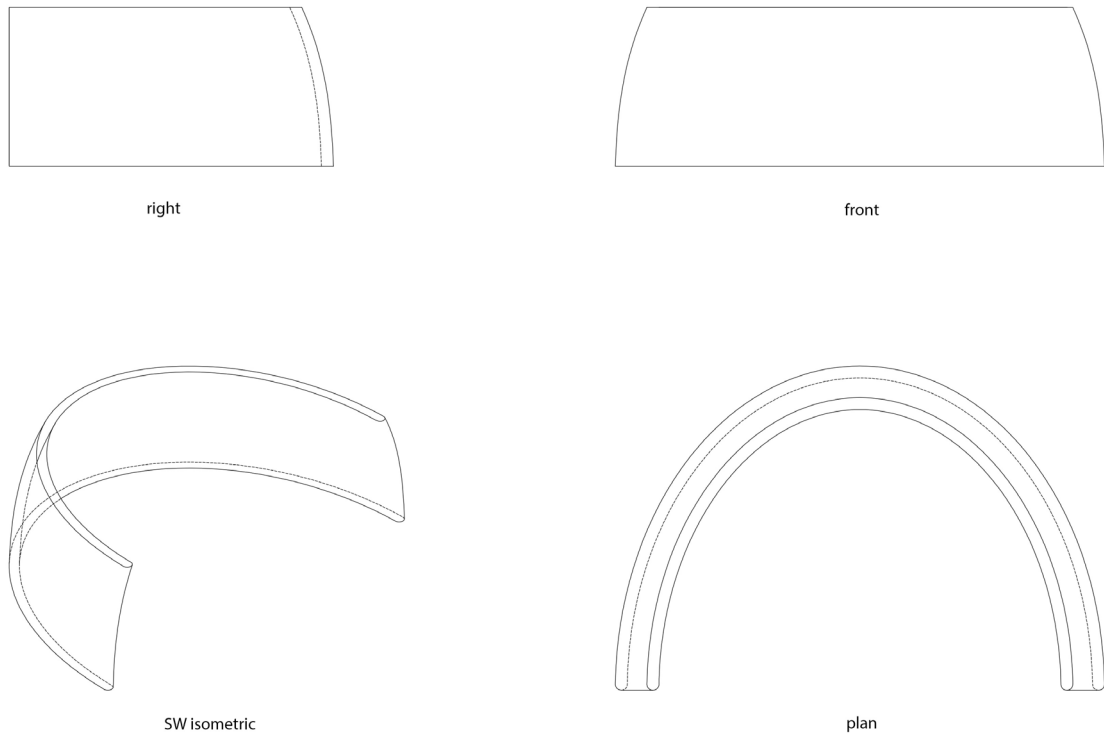
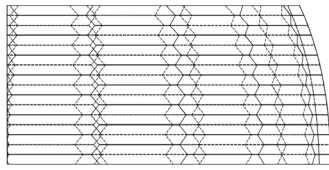
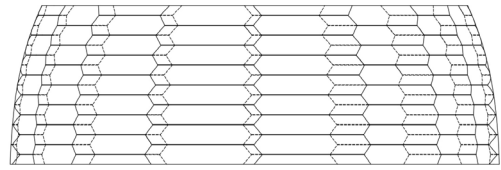


**Figure 33: Geometry of the demonstrator wall.**

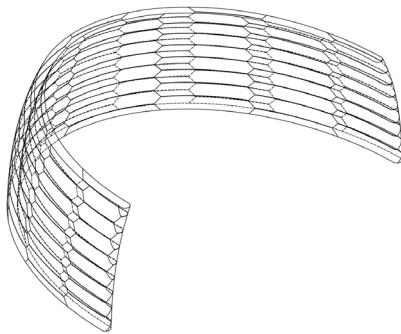
A hexagon tessellation pattern is applied to the formwork surface. On the ground plane, the footprint is split into 16 segments. The tile layer count is 25. The boundary tilt angle is 40 degrees.



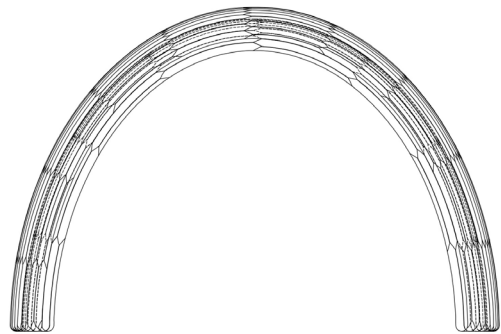
right



front



SW isometric



plan

**Figure 34: Hexagon tessellation applied to formwork surface of the wall.**

The next step is segmentation. The contour curves on each layer are split into segments and grouped into tiles.

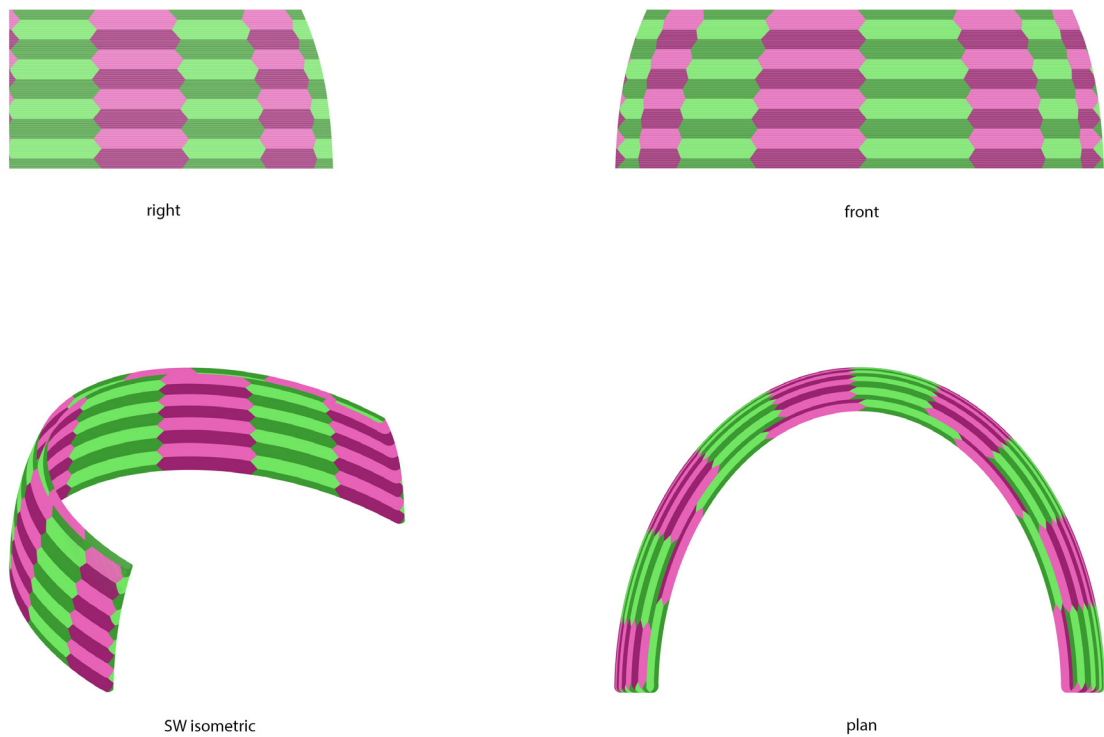


**Figure 35: Print path model of the wall after segmentation.**

Then, undulation is introduced to the print path. The undulation length and amplitude are set as 20 mm and 10 mm.

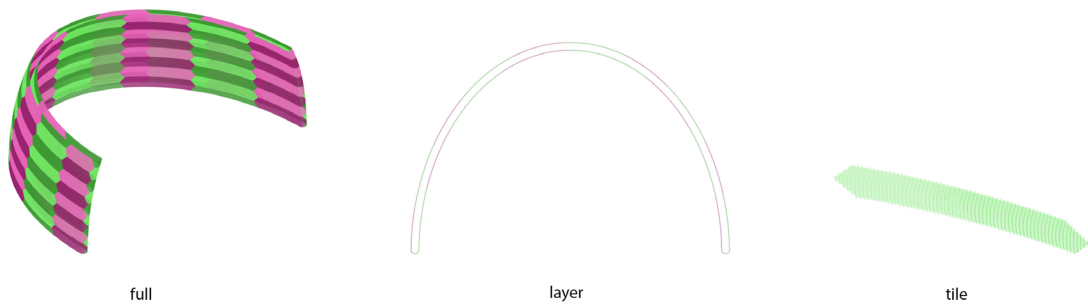


**Figure 36: Print path model of the wall after integrating undulation.**

Next, stiffeners are integrated into the print path. In this use case, the lengths of stiffeners are calculated based on the self-weight of the formwork. In addition to the previously mentioned calculation method, I also introduced a maximal overhang value to prevent the stiffeners from overhanging outwards too much. Because of this, the stiffeners on the outwards-tilting side of the wall are longer than the stiffeners on the inwards-tilting side. Different from

the print path of the column, the stiffener polylines are designed as a T-shape to increase stability.

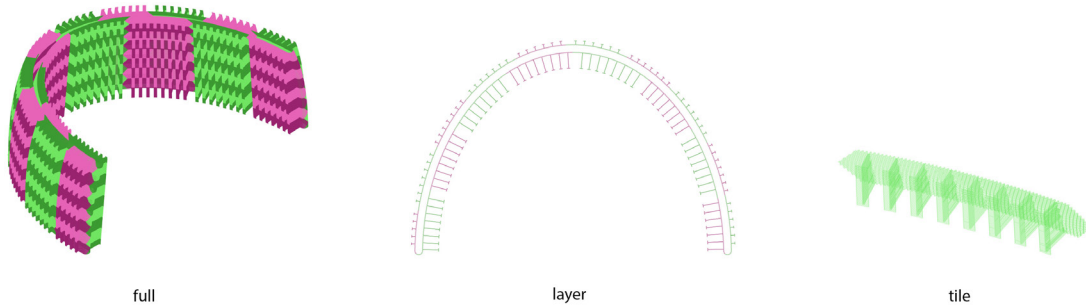


Figure 37: Print path model of the wall after integrating stiffeners.

At last, the end joints are integrated into the print path. The maximal overhang angle is set as 15 degrees.

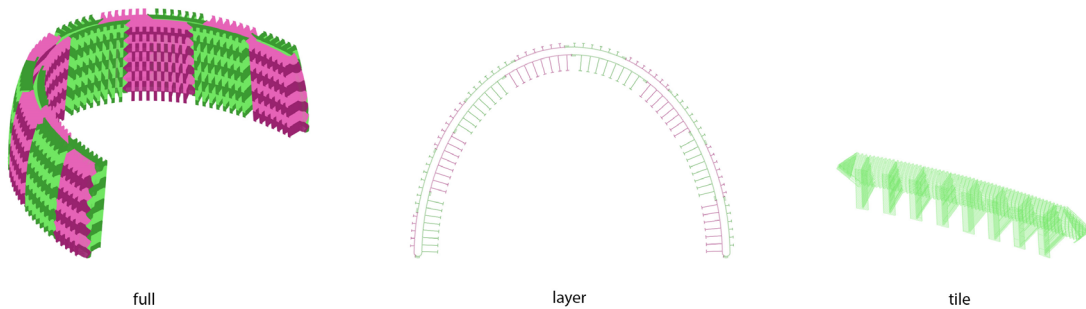


Figure 38: Final print path model of the wall after integrating joints.

### 5.3. Fabrication of The Column

The column designed in chapter 5.1 is fabricated with one mobile robot in 1:1 scale to evaluate the feasibility of the print path design. The column has a height of two meters. The print path has 400 layers in total. The whole clay formwork is segmented into 51 segments in a hexagon tessellation pattern, including 45 full segments and 6 half segments. Each full segment has a height of 25 centimetre and a print path with 50 layers.



Figure 39: Clay formwork of the column being printed. Photo credit: Gido Dielemans

The designed print path model is connected to a simulation and control environment in grasshopper. Based on the print path model, a sequence of spatial frames is created. The spatial frames indicate the position and posture of the robot end-effector and control the movement of the robot arm.

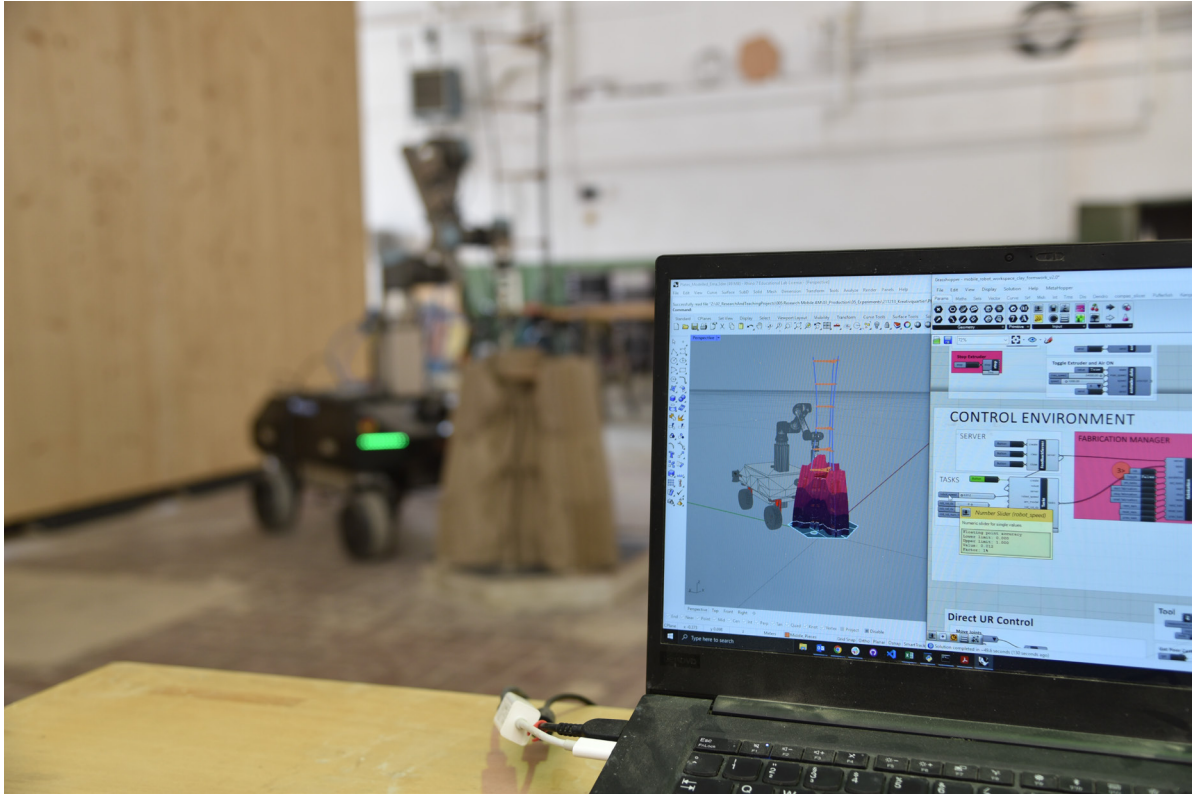


**Figure 40: Fabrication control in grasshopper. On the left side of the picture is the mobile robot printing a tile of the clay formwork. On the right side of the picture is the simulation and control environment in grasshopper. Photo credit: Gido Dielemans**

The water amount in the clay must be carefully controlled and the clay should be air-free. Before being able to be printed, clay must be well-prepared. First, clay and water are mixed thoroughly with a mixer. Then, the well-mixed clay is added into a Nidec NVA-04S vacuum pugmill. With this machine clay is filled into a plastic tube - the “cartridge”. Then, the cartridge is plug into a metal cartridge holder attached to the forearm of the robot.



**Figure 41: Clay being prepared. A bucket of clay is being mixed with water in the middle of the picture. The well-mixed clay is being filled into a cartridge with the vacuum pugmill on the left-down corner of the picture. Photo credit: Gido Dielemans**

The column is fabricated in a consecutive printing and casting process. In the case of this column, concrete is cast every time after we print three full formwork segments. In one print-cast-cycle, the height of clay formwork increases by 12.5 centimetres. The volume of concrete is calculated in the grasshopper model based on the shape of the column and the height increasement. The concrete we used is a fast-setting light-weight concrete developed at the Chair of Materials Science and Testing at the Technical University of Munich. In average, 5 to 6 tiles can be fabricated in a day. After 16 print-cast-cycles, the printing and casting of concrete column is complete. The incremental printing and casting strategy was proved successful.



**Figure 42: Clay formwork being printed. Picture credit: Gido Dielemans**

The stiffening and jointing features have been proved to be valid and important for the successful fabrication. The formwork is stable enough during the printing the casting process. And the increased contact surface between formwork tiles tolerated the inaccuracies caused by robot relocation.

The lower part of clay formwork began to lose water content and started to shrink already in the printing and casting process. The demoulding process did not cause much effort. The clay formwork tiles are recycled. The undulation and jointing of formwork become a visual feature of the fabrication process on the concrete surface.



Figure 43: Finished concrete column. The undulation of print path left a texture on the concrete surface. The joints also leave marks on the concrete. Picture credit: Gido Dielemans

## 6. Conclusio

This thesis aims at developing a 3D printed clay formwork for an in-situ fabrication scenario with mobile robots. The successful physical fabrication experiment proved the feasibility of printing clay formwork with mobile robots. The print path design strategies and the parametrical workflow have also been proven to be valid.

### 6.1. Outlook

As an outlook, functionalities such as openings can be integrated into the wall. The fabrication process of using segmented clay formwork opens possibilities of creative functional integration. For example, prefabricated door frame stones can be integrated during construction. The door frame stones can be produced using additive manufacture technologies such as selective cement activation. They replace one or more tiles of clay formwork during the printing and casting process as stay-in-place formwork.

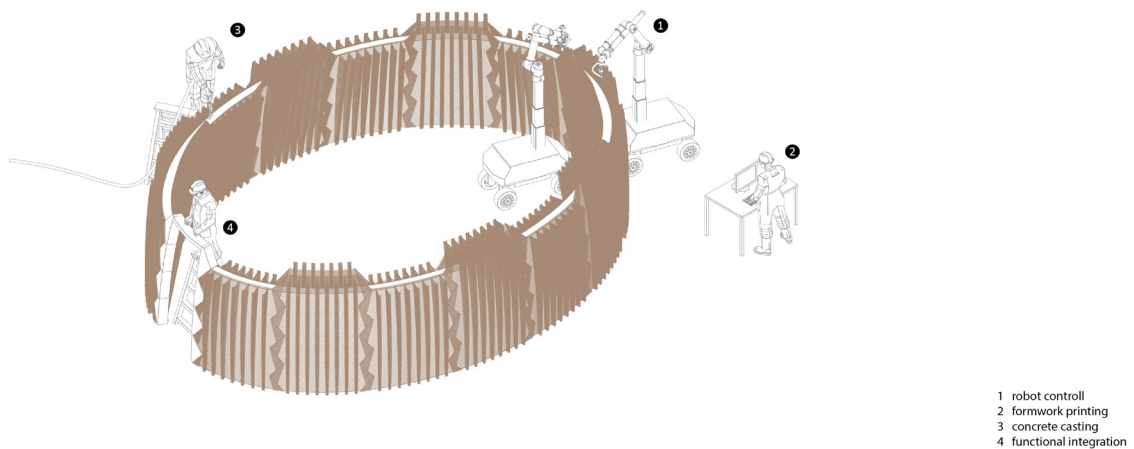


Figure 44: Fabrication scenario of an oval-shaped house using the methods developed in this thesis.

With the integration of functionality, the architectural application of this process is possible. Freeform load-bearing concrete structures such as walls and columns can be produced using this process. For example, an oval-shaped house can be fabricated using this technology. The 3D printed clay formwork leaves its texture on the concrete surface, which becomes a unique aesthetical feature.

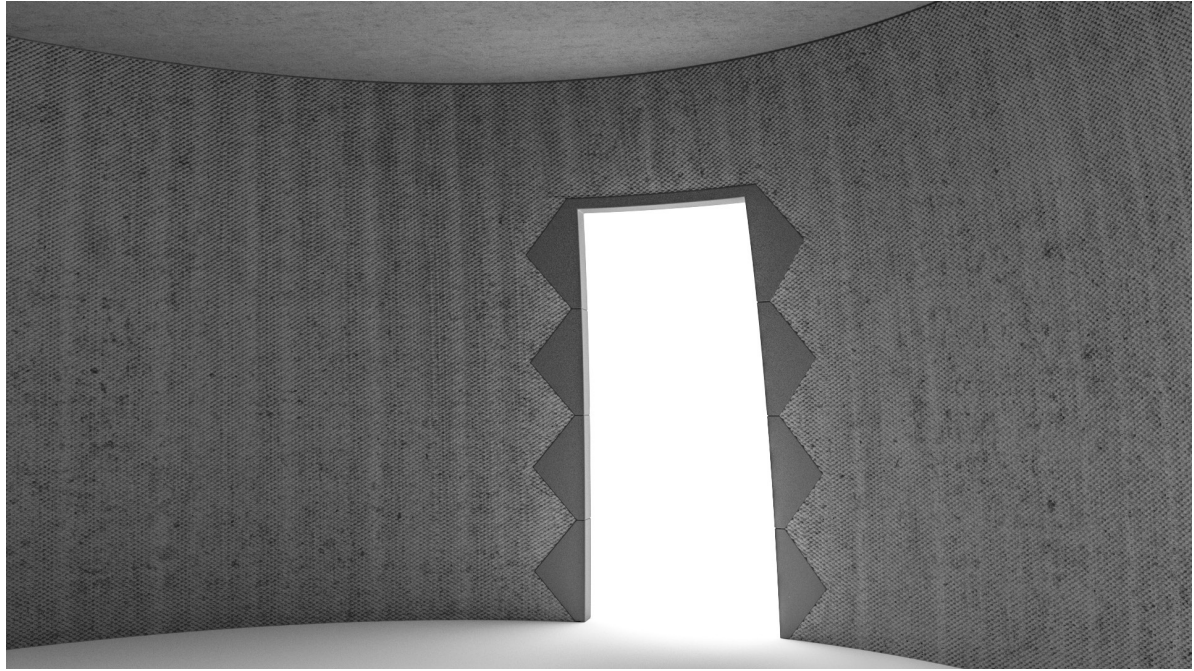


Figure 45: Visualization of a possible architectural application.

## 6.2. Discussion

In the experiment, we found out a significant difference in printability between our recycled clay and the new clay. Our recycled clay is printable at a density much lower than new clay, at which the clay material contains more water and has less structural ability. Clay also becomes more density-sensitive after recycling, meaning that the allowable density range is smaller than new clay. What exactly is the cause and how this phenomenon could be avoided needs to be investigated in further research.

In a way similar to how concrete structures are commonly produced through casting, structures can be produced with earth. Admixtures can be added to the earth, letting earth be able to be cast into formworks and hardens after a period. Despite its problem of shrinkage and lack of water resistance, earth as a building material has the advantages of big thermal mass, the ability to adjust air humidity, to absorb air pollutant, availability and reusability (Minke 2021). These advantages make earth stand out as healthier and more eco-friendly compared to concrete. The combination of 3D printed clay formwork and earth casting is an interesting topic. Earth and clay are one material, yet if and how these two technologies can work together stays open. Julian Trummer, Pinar Sel, Gido, and I did an initial experiment to explore the possibility to combine earth casting with 3D printed clay formwork. In the future, this combination and its design potentials can be further explored.

## 7. Bibliography

“3D Concrete Printing Expands to World Construction.” n.d. Accessed September 14, 2022. <https://worldarchitecture.org/architecture-news/cvzhp/3d-concrete-printing-expands-to-world-construction.html>.

“3D PRINTED CLAY FORMWORK FOR CONCRETE CASTING - YouTube.” n.d. Accessed May 23, 2022. [https://www.youtube.com/watch?v=aQa6tqXRXxM&list=TLPQMjMwNTIwMjKaND\\_rV9vkIQ&index=1&ab\\_channel=Kamon](https://www.youtube.com/watch?v=aQa6tqXRXxM&list=TLPQMjMwNTIwMjKaND_rV9vkIQ&index=1&ab_channel=Kamon).

Jipa, Andrei, and Benjamin Dillenburger. 2021. “3D Printed Formwork for Concrete: State-of-the-Art, Opportunities, Challenges, and Applications.” *3D Printing and Additive Manufacturing*. <https://doi.org/10.1089/3dp.2021.0024>.

Minke, Gernot. 2021. *Building with Earth: Design and Technology of a Sustainable Architecture*. Fourth. <https://doi.org/10.3362/9781780443959>.

“Print-Cast-Print - YouTube.” n.d. Accessed May 24, 2022. [https://www.youtube.com/watch?v=LWfy47vVuDo&ab\\_channel=TechZone](https://www.youtube.com/watch?v=LWfy47vVuDo&ab_channel=TechZone).

“Ruxin Xie - 21SU’ Cocoon.” n.d. Accessed April 30, 2022. <https://ruxinx.com/3d-printed-clay-formwork-for-concrete>.

“TEXT\_Qian Li and Kamon Nartnarumit - Taubman College Thesis 2022.” n.d. Accessed May 23, 2022. [https://taubmancollegethesis-2022.com/TEXT\\_Qian-Li-and-Kamon-Nartnarumit](https://taubmancollegethesis-2022.com/TEXT_Qian-Li-and-Kamon-Nartnarumit).

## 8. Table of Figures

Figure 1: Clay formwork being printed (left). Prototype of a 3D lattice structure (right). (“3D Concrete Printing Expands to World Construction” n.d.) .....	8
Figure 2: Incremental concrete casting process in “Cocoon” allows concrete to support the 3DP clay formwork (left). Concrete column “Cocoon” with branching geometry (right). (“Rcuxin Xie - 21SU’ Cocoon” n.d.) .....	8
Figure 3: Clay formwork being printed on top of previous cast (left). (“Print-Cast-Print - YouTube” n.d.) Concrete being casted in 3d printed clay formwork (right). (“3D PRINTED CLAY FORMWORK FOR CONCRETE CASTING - YouTube” n.d.) .....	9
Figure 4: In-situ clay formwork printing scenario. ....	10
Figure 5: Diagram of research method. ....	12
Figure 6: Illustration of terms for the segmentation.....	12
Figure 7: Maximal segment length in relation to footprint curvature and robot range. In illustration, the outer range has a radius of 0.6 meter and the inner range has a radius of one meter.....	13
Figure 8: First segment found with geometrical method on a footprint curve with variable curvature.....	14
Figure 9: Splitting points, robot ranges and robot positions found on a footprint curve with variable curvature. ....	15
Figure 10: Splitting points, robot ranges and robot positions found on a footprint curve with a tolerance parameter introduced.....	16
Figure 11: Initial geometries for the segmentation on the formwork surface. ....	17
Figure 12: Diagram of a consecutive printing and casting process. ....	18
Figure 13: Two strategies to avoid the end-effector collision. Left: tilted end-effector axis. Right: tilted tile boundary.....	18
Figure 14: Tessellation strategies.....	19
Figure 15: Splitting points found on layers of contour curves.....	20
Figure 16: Segmented contour curve regrouped into tiles according to the tessellation.....	22
Figure 17: Model of clay formwork before and after application of undulation. ....	23
Figure 18: Print path before and after application of undulation.....	24
Figure 19: Model of clay formwork before and after integration of stiffeners. ....	25
Figure 20: Physical model to calculate the stiffener length from the formwork tilt angle.....	26
Figure 21: Relation between the formwork tilt angle and the stiffener length required to avoid tipping over. The parameters used are listed next to the graph.....	27
Figure 22: Stiffener polyline created from the stiffener vector and integrated into the print path.....	28
Figure 23: Concept of jointing. ....	29
Figure 24: Print path before and after the integration of joints. ....	29
Figure 25: Locations for jointing details on a tile. ....	30
Figure 26: The print path of four tiles with and without integrated joints. ....	31
Figure 27: Geometry of the demonstrator column. ....	32
Figure 28: Hexagon tessellation applied to formwork surface of the column. ....	33
Figure 29: Print path model of the column after segmentation.....	34
Figure 30: Print path model of the column after integrating undulation. ....	35
Figure 31: Print path model of the wall after integrating stiffeners. ....	36
Figure 32: Final Print path model of the column after integrating joints. ....	37
Figure 33: Geometry of the demonstrator wall.....	38
Figure 34: Hexagon tessellation applied to formwork surface of the wall.....	39
Figure 35: Print path model of the wall after segmentation. ....	40
Figure 36: Print path model of the wall after integrating undulation. ....	40
Figure 37: Print path model of the wall after integrating stiffeners. ....	41
Figure 38: Final print path model of the wall after integrating joints. ....	41
Figure 39: Clay formwork of the column being printed. Photo credit: Gido Dielemans.....	42

Figure 40: Fabrication control in grasshopper. On the left side of the picture is the mobile robot printing a tile of the clay formwork. On the right side of the picture is the simulation and control environment in grasshopper. Photo credit: Gido Dielemans ..... 43

Figure 41: Clay being prepared. A bucket of clay is being mixed with water in the middle of the picture. The well-mixed clay is being filled into a cartridge with the vacuum pugmill on the left-down corner of the picture. Photo credit: Gido Dielemans ..... 44

Figure 42: Clay formwork being printed. Picture credit: Gido Dielemans ..... 45

Figure 43: Finished concrete column. The undulation of print path left a texture on the concrete surface. The joints also leave marks on the concrete. Picture credit: Gido Dielemans ..... 46

Figure 44: Fabrication scenario of an oval-shaped house using the methods developed in this thesis..... 47

Figure 45: Visualization of a possible architectural application. .... 48